

https://dspace.org/

Interactions in one dimension studied using the density matrix renormalization group

Boeyens, Julia

2020
https://hdl.handle.net/10539/31028

Downloaded from a DSpace repository. https://dspace.org/

Interactions in one dimension studied using the density matrix renormalization group

---

A dissertation submitted to the University of the Witwatersrand in fulfilment of the requirements for the degree of Master of Science. Johannesburg, 2019

Julia Boeyens* 715250

Faculty of Science, School of Physics

University of the Witwatersrand

Supervised by Dr. Izak Snyman†

* julia.boeyens@gmail.com

† izak.snyman@wits.ac.za

Declaration

I declare that this dissertation is my own, unaided work. It is being submitted for the Degree of Master of Science at the University of the Witwatersrand, Johannesburg. It has not been submitted before for any degree or examination at any other University.

Signed:  Date: June 29, 2020

Acknowledgements

I would like to thank my supervisor Dr. Izak Snyman for his patience and guidance in every stage of preparing the work for this dissertation. I would also like to thank the National Research Foundation of South Africa for their financial support of this research (Grant Number: 112332).

Abstract

In this dissertation, a density matrix renormalisation group program is developed, which is detailed and benchmarked for a spin chain with a Josephson junction. This program is then used to study interactions in a one-dimensional wire consisting of spinless, p-wave paired superconducting electrons. We study the effect that interactions have on the 4π Josephson effect by considering the degeneracies in the first few eigenstates of the Hamiltonian. It is found that the 4π Josephson effect is preserved up to finite size corrections, which indicates that particle hole symmetric interactions are not a source of quasiparticle poisoning. However, the finite size corrections decay slower than predicted by a non-interacting theory of the system with the same size gap. Thus, interactions affect the superconductivity in a way that is not accurately accounted for by an effective mean field theory.

List of Figures

2.2 The difference from the exact energies of the infinite system DMRG algorithm decreases for an increasing number of kept states D. Here, $\{W, \Delta, U\} = \{1.0, -0.2, 0\}$, the chain has 82 sites and there is no junction. The yellow line represents the difference in value between the first state in the band obtained from the DMRG program and the exact energy calculated. The red line represents the difference for the ground state and the blue line represents the difference for the second energy in the spectrum which should be degenerate with the ground state. 30

2.3 The difference from the exact energies of the infinite system DMRG algorithm decreases for an increasing number of kept states D. Here, $\{W, |\Delta|, U\} = \{1.0, 0.2, 0\}$, the chain has 82 sites and there is a Josephson junction with a different sign for the order parameter on each side. At the junction, $\{W, \Delta, U\} = \{1.0, 0, 0\}$. The green line depicts the difference in value between the energy calculated for the first state in the band using DMRG and the exact state. The same difference for the fourfold degenerate ground state energies are represented by the red, blue, orange and purple lines. 31

2.4 This diagram illustrates part of a sweep to the right during finite system DMRG. Initially, the superblock is built up with the junction in the middle using infinite system DMRG. The two sides of the junction have a π phase difference between them. This amounts to swapping the sign of Δ in the part of the chain that is shaded blue compared to the part that is shaded yellow. Once the system is built in this way sweeping begins. The diagram shows that as a sweep is performed, the choice of the parameters on either side of the joining of the superblock must change. 34

2.5 The accuracy of the calculation for the first state in the band is shown with respect to the number of kept states and the method of targetting. For this calculation, $\{W, |\Delta|, U\} = \{1.0, 0.2, 0\}$, the chain has 82 sites and there is a Josephson junction with a π phase difference between the two sides. At the Junction, $\{W, \Delta, U\} = \{1.0, 0, 0\}$. The red line shows the behaviour of the system when the band is not targetted, the blue line represents the behaviour when the first energy in the band is calculated but no state averaging is used and finally, the yellow line represents the performance of the DMRG calculation when the first state in the band is targetted and the state averaging method is applied. 36

3.1 The first 12 eigenenergies of the wire with a Josephson junction with a π phase difference across it. The system on either side of the junction has 41 sites and 56 states are kept at each DMRG truncation step. Four values of U are shown in terms of $U_{c\pm} = |W + \Delta|$. The two panels in the centre show the behaviour for the intrinsically gapped phase and the outer two panels show the extrinsically gapped phase. Finite size effects are more apparent for $U > 0$ as shown by the degeneracy of the ground and excited states lifting. 42

3.3 The difference from the ground state energy for the first four excited states was calculated as a function of increasing system size. The decay was fit with an exponential function of N depicted by the grey lines. 44

List of Tables

2.1 The array in Eq. 2.10 has a block diagonal structure that emerges when it is represented in two dimensions. H_N and S_N^i with $i \in \{x, y, z\}$ denote the Hamiltonian and spin matrices for the matrix before the addition of the site. The indices α and β are used to index matrix H_N and a and b both run over $\{1, 2\}$ as they index the two degrees of freedom of the added site. 14

Contents

Declaration i
Aknowledgements ii
Abstract iii
List of Figures iv
List of Tables vi

1 Introduction **1**

2 The density matrix renormalisation group method **11**
2.1 Truncation of the basis 17
2.2 DMRG implementation for the Heisenberg chain 20
2.2.1 Adding a site to the existing chain and building the superblock 21
2.2.2 Diagonalising the superblock 22
2.2.3 Creating the reduced density matrix of the system 24
2.2.4 Truncating the operators using the new basis 25
2.3 Exact Diagonalization of the Hamiltonian with no interactions . . 25
2.3.1 Performance of the DMRG code 29
2.4 The effect of building the system in a different environment 29
2.5 Finite system DMRG 32
2.6 Calculation of excited states 34

3 Zero-energy quasiparticles in an interacting nanowire containing a topological Josephson junction **37**
3.1 MZMs in the presence of interactions 40

4 Conclusions **46**

References **51**

A Properties of the Pauli matrices **52**

B Anti-commutation relation of the BdG operators **55**

C Commutation of Majorana operators with the non-interacting Hamiltonian **57**

1 Introduction

Developing and using many-body techniques to understand the behaviour of interacting quantum systems at finite particle density is one of the largest areas of research in condensed matter physics. In some systems, the problem can be simplified by ignoring the Coulomb interactions in the system or including them perturbatively. This is possible because the Coulomb interactions are effectively screened by the electron plasma. These systems can then be described with a single-particle Hamiltonian using an effective mean field theory. However, there are systems where the effective interaction is not weak enough to make these approximations and the system has to be solved as a many-body problem. These systems are known as strongly correlated systems and many of them give rise to interesting physics [1]. It is particularly important to include interactions in one-dimensional systems where they often give rise to phenomena that do not exist in higher dimensions [2].

This dissertation has two aims. The first aim is to present my own implementation of a numerical technique known as the density matrix renormalisation group (DMRG). This method provides a way to study large, strongly correlated, low dimensional systems to a high precision [1]. The second aim is to show the results obtained by applying this method to a system of current interest.

Producing a DMRG program is non-trivial. Even a minimal implementation will typically contain thousands of lines of code. The method was developed in the early 1990's and since then versatile open source programs have been created. Most practitioners that wish to use DMRG will employ one of these open source software packages. However, the aim of this project was not to simply use one

of these programs as a black box method to obtain the energies and expectation values of interacting systems. Rather, the aim was to understand the many-body physics behind the method. To this end, I decided to develop my own DMRG program the source code of which can be found on Zenodo [3]. The program I have written works for spin 1/2 chains with nearest neighbour couplings. This class of systems is a very small subset of the systems that can be studied using DMRG. However, it contains systems that have been studied intensively in recent years and illustrates all of the essential components of a DMRG program.

Chapter 2 contains the details of how the DMRG program used in this dissertation was developed. This chapter is intended as a guide for those who want to learn DMRG. It focusses on applying DMRG to the spin chain which is a simple but instructive problem. It complements the excellent reviews [1, 4] that give a more general formulation of DMRG but do not go into the low-level technical details of how to write a DMRG program. In Chapter 3, DMRG is used to reveal the existence of zero energy quasiparticles in an interacting nanowire. These quasiparticles have lifetimes that tend to infinity exponentially as the system size increases. This is an interesting result because usually quasiparticles in interacting systems have finite lifetimes. The work presented in this chapter also forms part of a recently posted preprint [5] that has been submitted to Physical Review B. The system studied in Chapter 3 informs the choices made about how the DMRG program is implemented in Chapter 2. We therefore close the introduction to this dissertation with an introduction to the problem that is discussed further in Chapter 3.

The system studied in this dissertation is a one-dimensional superconducting nanowire with strong spin-orbit coupling. The superconductivity in the wire is induced by its contact with a bulk superconductor. Many superconducting systems are well described by using an effective mean field theory for Cooper pairing interactions between the electrons. Hence, the fundamental degrees of freedom in the system are Bogoliubov quasiparticles [6]. The bulk superconductor is a good example of such a system.

The attractive interactions between Cooper pairs in this wire are exactly described by terms in the Hamiltonian that are quartic in creation and annihilation operators.

This makes the Hamiltonian impossible to solve by exact diagonalisation for large systems because of the exponential growth of the Hilbert space. Thus, a mean field approach is used. The operator $a_{k,\sigma}a_{k',\sigma'}$ that annihilates a Cooper pair with momentum k and spin σ can be written as

$$a_{k,\sigma}a_{k',\sigma'} = \langle a_{k,\sigma}a_{k',\sigma'}\rangle + d(a_{k,\sigma}a_{k',\sigma'}), \tag{1.1}$$

which is simply the sum of its mean value $\langle a_{k,\sigma}a_{k',\sigma'}\rangle$ and small fluctuations $d(a_{k,\sigma}a_{k',\sigma'})$ around that mean. Then, the mean field approximation comes from neglecting all terms in the Hamiltonian that are quadratic in the fluctuations. Thus, the Hamiltonian is quadratic in creation and annihilation operators and it can be solved using the Bogoliubov de Gennes equation [6].

The bulk superconductor screens most of the intrinsic Coulomb interactions between the electrons and induces superconductivity in the nanowire. However, it does not necessarily screen the short range part of the Coulomb interactions [7, 8, 9, 10, 11]. These interactions in the nanowire may not be effectively described by a mean field approach, like the one used to describe Cooper pairs, because it is a one-dimensional system [2]. If this is the case, the occupation numbers of the quasiparticle orbitals are not conserved and the system must be treated as a non-trivial, interacting many-body system.

These repulsive interactions between electrons on adjacent sites in the lattice would be described by terms involving quadratic products of the number operator, like $n_j n_{j+1}$, in the Hamiltonian. The mean field approach is then to set $n_j n_{j+1} = [\langle n_j\rangle + dn_j][\langle n_{J+1}\rangle + dn_{j+1}]]$ and exclude contributions that are quadratic in the fluctuations about the mean values. Once again, the Hamiltonian can now be solved. The prediction that is made by this solution is that for arbitrarily small interaction strengths there will be a gap in the energy spectrum. However, more careful calculations, using a renormalization group approach, show that there is a gap only when the absolute value of the interaction strength is larger than the hopping amplitude [12].

The superconductivity that is induced in the nanowire is of an unusual kind. It is known as "spinless" p-wave superconductivity. The bulk superconductor

displays usual s-wave pairing. In this type of superconductivity, the Cooper pairs form between electrons of opposite spin in a spin singlet. That is, the part of the Hamiltonian that will describe the Cooper pairs is

$$\sum_{j,k} \Delta_{j-k}(a_{j\uparrow}a_{k\downarrow} - a_{j\downarrow}a_{k\uparrow}) + \text{h.c.}, \tag{1.2}$$

where, $a^{\dagger}_{j\uparrow}$ is the fermionic creation operator that creates an electron with spin up on site j, Δ_{j-k} gives the distance dependent superconducting pairing amplitude and h.c. denotes the Hermitian conjugate. Now, consider two terms in this sum when $j = a,\ k = b$ and $j = b,\ k = a$,

$$\begin{aligned} &\Delta_{a-b}(a_{a\uparrow}a_{b\downarrow} - a_{a\downarrow}a_{b\uparrow}) + \Delta_{b-a}(a_{b\uparrow}a_{a\downarrow} - a_{b\downarrow}a_{a\uparrow}) \\ =&\Delta_{a-b}(a_{a\uparrow}a_{b\downarrow} - a_{a\downarrow}a_{b\uparrow}) + \Delta_{b-a}(-a_{a\downarrow}a_{b\uparrow} + a_{a\uparrow}a_{b\downarrow}) \\ =&(\Delta_{a-b} + \Delta_{b-a})(-a_{a\downarrow}a_{b\uparrow} + a_{a\uparrow}a_{b\downarrow}). \end{aligned} \tag{1.3}$$

The second last line follows from the fermionic anti-commutation relations. Without loss of generality, we can choose $\Delta_{a-b} = \Delta_{b-a}$. Thus, the order parameter is even. On the other hand, p-wave pairing has an odd order parameter because the spin configuration is symmetric under exchange. In the system we consider, this is achieved by effectively getting rid of the spin degree of freedom. For this to be possible, the nanowire must be made of a material with strong spin orbit coupling. This will result in a splitting in the energy spectrum according to the polarization of the spin of the electrons. However, the spectrum will still be degenerate. When a Zeeman field perpendicular to the direction of the spin-orbit field is turned on, it results in the opening of a gap. Inside this gap there is no spin degeneracy [13]. Thus, for low energy electrons, the direction of the spins is fixed and thus, they are chiral [14]. Without a spin degree of freedom, the Cooper pairing term reads

$$\sum_{j,k} \Delta_{j-k}a_j a_k + \text{h.c.} \tag{1.4}$$

The terms with $j = a,\ k = b$ and $j = b,\ k = a$ are

$$\begin{aligned} &\Delta_{a-b} a_a a_b + \Delta_{b-a} a_b a_a \\ =&\Delta_{a-b} a_a a_b - \Delta_{b-a} a_a a_b \\ =&(\Delta_{a-b} - \Delta_{b-a}) a_a a_b, \end{aligned} \tag{1.5}$$

where, the fermionic anti-commutation relation was used in the second last line. Without loss of generality, we can set $\Delta_{a-b} = -\Delta_{b-a}$. This means the pairing is odd.

In the last decade, one-dimensional nanowires with spinless p-wave superconductivity have been studied intensively [15]. These wires host two spatially separated Majorana bound states that are localised at the ends of the wire. These bound states are discussed explicitly in Chapter 3. The bound states give rise to a zero energy quasiparticle orbital [13, 14, 16, 17]. Each energy level of this system is then two fold degenerate because it requires no additional energy to fill or empty the zero energy orbital. This property may make such systems promising candidates for the production of self correcting quantum memory [13, 18]. In order to process quantum information in a fault free way, the proposed technique involves braiding of states.

A braiding operation is a unitary operation that exchanges two particles. Usually, two exchanges of the same two particles will leave the system invariant. However, this is not the case for Majorana fermions. In this case, the positions will be the same but the state will not. The detailed technicalities of quantum information processing in this way are beyond the scope of this dissertation. It suffices to say that the controlled manipulation of quantum information using braiding requires quasiparticles with creation and annihilation operators that are built from two Majorana operators. These must be localized near opposite ends of the wire. If these operators commute with the Hamiltonian, the Hilbert space can be factored into a tensor product of the localized two-level system, which consists of the quasiparticle orbital that is either empty or full, with the Hilbert space of the rest of the degrees of freedom in the system. Therefore, there is no coupling between the two level system and the bulk degrees of freedom even in the presence of short range electron-electron interactions.

It has been found that the spinless p-wave nanowire that supports localized quasiparticle orbitals is topologically non-trivial. This means it belongs to a topological phase of matter that is characterised not by its symmetry, as many phases of matter are, but rather by its topological order [19]. In the one dimensional nanowire with a gapped ground state manifold, the ground state degeneracy has the robustness of a topological invariant. Only perturbations strong enough to close the gap can change it [20]. This robustness is known as topological protection [21, 22, 23, 24].

Topological protection of the ground state degeneracy ensures it is present even when short range interactions are included. However, to the best of my knowledge this does not imply that, in the presence of interactions, Majorana operators exist that produce the localized quasiparticle orbitals that produce the twofold *spectral* degeneracy known as strong Majorana zero modes. In fact, one of the experts in the field, Paul Fendley, has said, "The strong zero mode pairs each state in the even-fermion-number sector with one in the odd, requiring their energies are the same up to exponentially small finite-size corrections. It therefore results in a much stronger constraint on the energy spectrum than the constraint of topological order, where only pairing of ground states is necessary" [25].

However, if only the ground state is degenerate, quasiparticle excitations in the bulk can destroy information that is stored in the degenerate ground states. That is, immediately after preparing the initial state the system may seem to be in the desired state belonging to the true ground state manifold. However, the system has very many degrees of freedom and so there may be a single accidental quasiparticle excitation in the bulk far from the edge. This excitation is a linear combination of excited states. Therefore, as the system is allowed to evolve in time, the excitation may propagate to the ends. This would induce a non-trivial time evolution of the state that is being used to store the quantum information. This destroys the information that was encoded on the state. This process is known as quasiparticle poisoning.

Fendley showed that in a spinless p-wave wire, like the one studied here, Majorana operators can be constructed for the end states of the wire when particle-hole symmetric interactions are included. The existence of these operators implies

that in fact full twofold spectral degeneracy is preserved. Thus, in this system, electron-electron interactions do not lead to quasiparticle poisoning.

In Chapter 3, Fendley's results are extended to a system where the superconducting order parameter varies in space. To be more precise, a Josephson junction will be introduced into the wire and we will investigate the situation when the order parameter changes sign at the junction. We provide the motivation for this extension at the start of Chapter 3. Here, we make the definitions required to discuss the implementation of DMRG for the system of interest. The model that we study consists of a one-dimensional lattice with $2N$ sites. We write the Hamiltonian as

$$H_{2N} = H_{2N,0} + H_{2N,\text{int}}, \tag{1.6}$$

where $H_{2N,0}$ is the part of the Hamiltonian that is describes the p-wave superconducting and hopping between sites in the absence of interactions and $H_{2N,\text{int}}$ describes particle hole symmetric short-range interactions. These are each given explicitly by

$$\begin{aligned} H_{2N,0} = &- \frac{W}{2}\sum_{j=1}^{2N-1}(a_j^\dagger a_{j+1} + a_{j+1}^\dagger a_j) \\ &+ \frac{\Delta}{2}\sum_{j=1}^{N-1}(a_j a_{j+1} + a_{j+1}^\dagger a_j^\dagger) \\ &- \frac{\Delta}{2}\sum_{j=N+1}^{2N-1}(a_j a_{j+1} + a_{j+1}^\dagger a_j^\dagger) \end{aligned} \tag{1.7}$$

and

$$H_{2N,\text{int}} = U\sum_{j=1}^{2N-1}(n_j - \frac{1}{2})(n_{j+1} - \frac{1}{2}). \tag{1.8}$$

Here, Δ is the superconducting order parameter, $W/2$ is the hopping amplitude and U is the interaction strength. The operators a_j and $a_j^\dagger$ define the fermionic annihilation and creation operators for the electron on site j and $n_j = a_j^\dagger a_j$ is the number operator.

The DMRG program implemented in this dissertation works for spin 1/2 chains and so the Jordan Wigner transformations are used to map this Hamiltonian

given in terms of fermionic operators to one in terms of Pauli matrices. The transformations are given by [26]

$$\begin{aligned}\sigma_j^x &= \prod_{k=1}^{j-1}(2n_k-1)(a_j+a_j^\dagger)\\ \sigma_j^y &= \prod_{k=1}^{j-1}(2n_k-1)i(a_j-a_j^\dagger)\\ \sigma_j^z &= 2n_j-1. \end{aligned} \tag{1.9}$$

The Pauli matrices defined in this way have the usual properties,

$$\begin{aligned}&(\sigma_j^x)^2=(\sigma_j^y)^2=(\sigma_j^z)^2=1\\ &\sigma_j^x\sigma_j^y=i\sigma_j^z\\ &[\sigma_j^x,\sigma_k^y]=[\sigma_j^x,\sigma_k^z]=[\sigma_j^y,\sigma_k^z]=0, \quad \text{if } \ j\neq k. \end{aligned} \tag{1.10}$$

These properties are explicitly proved in Appendix A.

The terms in the non-interacting part of the Hamiltonian involve quadratic products of creation annihilation operators on different sites. Therefore, consider

$$\sigma_j^x\sigma_{j+1}^x=\prod_{k=1}^{j-1}(2n_k-1)(a_j+a_j^\dagger)\prod_{k=1}^{j}(2n_k-1)(a_{j+1}+a_{j+1}^\dagger). \tag{1.11}$$

Since $(2n_l-1)^2=1$ and $[n_l,a_m]=0$, when $l\neq m$,

$$\begin{aligned}\sigma_j^x\sigma_{j+1}^x &= (a_j+a_j^\dagger)(2n_j-1)(a_{j+1}+a_{j+1}^\dagger)\\ &= (a_j-a_j^\dagger)(a_{j+1}+a_{j+1}^\dagger),\end{aligned} \tag{1.12}$$

where, the last line follows because $a_jn_j=a_j$ and $a_j^\dagger n_j=0$. By multiplying out the brackets, one obtains,

$$\begin{aligned}\sigma_j^x\sigma_{j+1}^x &= -a_j^\dagger a_{j+1}-a_j^\dagger a_{j+1}^\dagger+a_ja_{j+1}+a_j^\dagger a_{j+1}^\dagger\\ &= -(a_j^\dagger a_{j+1}+a_{j+1}^\dagger a_j)+(a_ja_{j+1}+a_{j+1}^\dagger a_j^\dagger).\end{aligned} \tag{1.13}$$

Similarly,

$$\sigma_j^y \sigma_{j+1}^y = -(a_j^\dagger a_{j+1} + a_{j+1}^\dagger a_j) - (a_j a_{j+1} + a_{j+1}^\dagger a_j^\dagger). \tag{1.14}$$

Then the sum of these operators is

$$\sigma_j^x \sigma_{j+1}^x + \sigma_j^y \sigma_{j+1}^y = -2(a_j^\dagger a_{j+1} + a_{j+1}^\dagger a_j) \tag{1.15}$$

and their difference is

$$\sigma_j^x \sigma_{j+1}^x - \sigma_j^y \sigma_{j+1}^y = 2(a_j a_{j+1} + a_{j+1}^\dagger a_j^\dagger). \tag{1.16}$$

Therefore, the non-interacting part of the Hamiltonian in terms of spin operators is

$$\begin{aligned} H_{2N_0} =& \frac{W}{4} \sum_{j=1}^{2N-1} (\sigma_j^x \sigma_{j+1}^x + \sigma_j^y \sigma_{j+1}^y) \\ &+ \frac{\Delta}{4} \sum_{j=1}^{N-1} (\sigma_j^x \sigma_{j+1}^x - \sigma_j^y \sigma_{j+1}^y) \\ &- \frac{\Delta}{4} \sum_{j=N+1}^{2N-1} (\sigma_j^x \sigma_{j+1}^x - \sigma_j^y \sigma_{j+1}^y). \end{aligned} \tag{1.17}$$

The interacting part of the Hamiltonian is easily obtained since

$$\sigma_j^z \sigma_{j+1}^z = \frac{1}{4}(n_j - \frac{1}{2})(n_{j+1} - \frac{1}{2}) \tag{1.18}$$

and thus,

$$H_{2N_{\text{int}}} = \frac{U}{4} \sum_{j=1}^{2N-1} \sigma_j^z \sigma_{j+1}^z. \tag{1.19}$$

The form that is most convenient for use in Chapter 2 is where the Hamiltonian resembles the XYZ Heisenberg model and is divided up into all the terms to the left of the junction, at the junction and to the right of the junction. The XYZ Heisenberg model for a chain of N spins is

$$H_N = \sum_{j=1}^{N-1} J_x \sigma_j^x \sigma_{j+1}^x + J_y \sigma_j^y \sigma_{j+1}^y + J_z \sigma_j^z \sigma_{j+1}^z. \tag{1.20}$$

The $2N$ site Hamiltonian in the form that will be used in Chapter 2 in the implementation of DMRG in terms of spin operators is then

$$\begin{aligned} H_{2N} = &\sum_{j=1}^{N-1}\left[\frac{W+\Delta}{4}\sigma_j^x\sigma_{j+1}^x + \frac{W-\Delta}{4}\sigma_j^y\sigma_{j+1}^y + \frac{U}{4}\sigma_j^z\sigma_{j+1}^z\right] \\ &+ \left[\frac{W}{4}\sigma_N^x\sigma_{N+1}^x + \frac{W}{4}\sigma_N^y\sigma_{N+1}^y + \frac{U}{4}\sigma_N^z\sigma_{N+1}^z\right] \\ &+ \sum_{j=N+1}^{2N-1}\left[\frac{W-\Delta}{4}\sigma_j^x\sigma_{j+1}^x + \frac{W+\Delta}{4}\sigma_j^y\sigma_{j+1}^y + \frac{U}{4}\sigma_j^z\sigma_{j+1}^z\right]. \end{aligned} \tag{1.21}$$

2 The density matrix renormalisation group method

The main results obtained in this work come from solving for the ground state of a modified version of the XYZ Heisenberg model. The equivalence of this model to the fermionic model was discussed at the end of Chapter 1. From the transformation done there we obtain the following relations between the couplings of the fermionic chain and the usual spin couplings in the spin chain

$$J_x = \frac{W+\Delta}{4}, \quad J_y = \frac{W-\Delta}{4}, \quad J_z = \frac{U}{4}. \tag{2.1}$$

These couplings will be used somewhat interchangeably according to which is more convenient. The values used in all numerical calculations will be given in terms of the fermionic $\{W, \Delta, U\}$ as this will make more sense for the results in Chapter 3 but some calculations and formulae are simplified by using $\{J_x, J_y, J_z\}$.

In order to introduce the DMRG method in a clear way, we focus on a chain in which the couplings are not position dependent. However, later in the chapter we allow for position dependence in the model. This will facilitate the study of the interacting system with a junction in Chapter 3. The XYZ model is given by the Hamiltonian

$$H_M = \sum_{j=1}^{M-1} J_x \sigma_j^x \sigma_{j+1}^x + J_y \sigma_j^y \sigma_{j+1}^y + J_z \sigma_j^z \sigma_{j+1}^z. \tag{2.2}$$

This Hamiltonian is for an M site chain. The coupling constants J_x, J_y and J_z are real valued and σ^x, σ^y and σ^z denote the Pauli matrices.

To build up to a DMRG program that will solve this model for an $2N$ site

chain, consider first the smallest non-trivial spin chain. That is, one with two sites given by

$$H_2 = J_x\sigma_1^x\sigma_2^x + J_y\sigma_1^y\sigma_2^y + J_z\sigma_1^z\sigma_2^z. \tag{2.3}$$

This is the smallest non-zero Hamiltonian. The Hamiltonian of a single site is zero because the model Hamiltonian has no terms that contain only a single site. With the goal of producing a computer program that will solve such a system, Eq. 2.3 needs to be represented in a way that a computer can utilise. We therefore represent the equation in matrix form by performing the following Kronecker products:

$$J_x\sigma_1^x \otimes \sigma_2^x = J_x \begin{pmatrix} 0 & 1 \\ 1 & 0 \end{pmatrix} \otimes \begin{pmatrix} 0 & 1 \\ 1 & 0 \end{pmatrix} = \begin{pmatrix} 0 & 0 & 0 & J_x \\ 0 & 0 & J_x & 0 \\ 0 & J_x & 0 & 0 \\ J_x & 0 & 0 & 0 \end{pmatrix} \tag{2.4}$$

$$J_y\sigma_1^y \otimes \sigma_2^y = J_y \begin{pmatrix} 0 & i \\ -i & 0 \end{pmatrix} \otimes \begin{pmatrix} 0 & i \\ -i & 0 \end{pmatrix} = \begin{pmatrix} 0 & 0 & 0 & -J_y \\ 0 & 0 & J_y & 0 \\ 0 & J_y & 0 & 0 \\ -J_y & 0 & 0 & 0 \end{pmatrix} \tag{2.5}$$

and

$$J_x\sigma_1^x \otimes \sigma_2^x = J_z \begin{pmatrix} 1 & 0 \\ 0 & -1 \end{pmatrix} \otimes \begin{pmatrix} 1 & 0 \\ 0 & -1 \end{pmatrix} = \begin{pmatrix} J_z & 0 & 0 & 0 \\ 0 & -J_z & 0 & 0 \\ 0 & 0 & -J_z & 0 \\ 0 & 0 & 0 & J_z \end{pmatrix}. \tag{2.6}$$

By adding these matrices together, the Hamiltonian is thus,

$$H_2 = \begin{pmatrix} J_z & 0 & 0 & J_x - J_y \\ 0 & -J_z & J_x + J_y & 0 \\ 0 & J_x + J_y & -J_z & 0 \\ J_x - J_y & 0 & 0 & J_z \end{pmatrix}. \tag{2.7}$$

The ground state of this system is easy to find because this matrix is small enough to be diagonalised exactly. However, a two site chain is far from the size required to reach the thermodynamic limit and so a larger chain must be built. In general, if we wanted to build the system up we could do this iteratively by adding sites to the chain. This procedure will now be outlined.

The Hamiltonian with $N+1$ sites H_{N+1} would be given in terms of the Hamiltonian for the N site chain H_N by

$$H_{N+1} = H_N \otimes \mathbb{1}_{2\times 2} + \sum_{i\in\{x,y,z\}} J_i S_N^i \otimes \sigma^i. \tag{2.8}$$

Here, $\otimes$ represents the Kronecker product, $\mathbb{1}_{2\times 2}$ is the two by two identity matrix, and the S_N^i are the spin operators for site N. For example, the operator S_N^z is given by

$$S_N^z = \mathbb{1}_{2^{N-1}\times 2^{N-1}} \otimes \sigma^z. \tag{2.9}$$

It will be more convenient, for the purposes of the algorithm, to give this matrix in terms of its matrix elements

$$H_{N+1_{(\alpha a)(\beta b)}} = H_{N_{\alpha\beta}}\delta_{a,b} + \sum_{i\in\{x,y,z\}} J_i S^i_{N_{\alpha\beta}} \sigma^i_{ab}, \tag{2.10}$$

where, $\delta_{a,b}$ is the Kronecker delta. The array H_{N+1} is indexed by four indices and shaped into a matrix. If matrix H_N is $L \times L$ dimensional, then H_{N+1} will have dimensions $2L \times 2L$. The indices α and β are used to index matrix H_N and a and b both run over $\{1, 2\}$ as they index the degree of freedom of the added site. The array H_{N+1}, as illustrated in Table 2.1, has a block diagonal structure when it is arranged into matrix form.

This structure makes diagonalization computationally less expensive because it allows for the use of efficient diagonalization subroutines. Thus, this matrix can be solved exactly for a few sites. However, since the dimensions double with the addition of a site at each step in the procedure, it becomes too large to diagonalise long before the system reaches the thermodynamic limit. For this reason, it is necessary to introduce an approximation that will allow the size of the system to grow but still ensures that the matrices remain at a manageable size.

	β	$1 \cdots L$	$1 \cdots L$
α		$b = 1$	$b = 2$
1 $\vdots$ L	$a = 1$	$H_{N_{\alpha,\beta}} + J_z S^z_{N_{\alpha,\beta}}$	$J_x S^x_{N_{\alpha,\beta}} - iJ_y S^y_{N_{\alpha,\beta}}$
1 $\vdots$ L	$a = 2$	$J_x S^x_{N_{\alpha,\beta}} + iJ_y S^y_{N_{\alpha,\beta}}$	$H_{N_{\alpha,\beta}} - J_z S^z_{N_{\alpha,\beta}}$

Table 2.1: The array in Eq. 2.10 has a block diagonal structure that emerges when it is represented in two dimensions. H_N and S^i_N with $i \in \{x, y, z\}$ denote the Hamiltonian and spin matrices for the matrix before the addition of the site. The indices α and β are used to index matrix H_N and a and b both run over $\{1, 2\}$ as they index the two degrees of freedom of the added site.

The method that is used to perform this calculation in the thermodynamic limit is DMRG. This method was developed from ideas pioneered by Wilson in his numerical renormalisation group (NRG) [27]. NRG was first used to solve impurity systems, In this method, the continuous Hamiltonian that is defined for the conduction band coupled to an impurity is made discrete. This is done by dividing up the energies of the conduction band into intervals making each interval exponentially smaller. The Hamiltonian which is now discrete in the energy is mapped to a chain Hamiltonian where each energy layer is a site of the chain. This chain Hamiltonian starts out describing the system for the impurity coupled to one site in the conduction band and, at each step of the renormalization procedure, a site is added to the chain and the Hamiltonian is diagonalized [28].

However, for each site that is added, additional degrees of freedom are added to the Hilbert space. Very quickly, the matrices that must be diagonalized become unmanageably large. Therefore, a truncation procedure is defined where, at each step, the eigenvectors of the Hamiltonian with largest eigenvalues are discarded so that the size of the Hilbert space remains constant. This truncation is physically

justified because the choice of the discretization ensures that states with higher energies do not have a marked effect on the low energy behaviour of the system [28]. After truncation, the operators are scaled and a new basis in terms of the lowest lying states is formed as well as an effective Hamiltonian for that energy scale. The procedure is repeated until the thermodynamic limit is reached.

It was hoped that the NRG procedure, which found so much success in impurity models, could be applied to real space systems [29]. In a real space formulation, the aim is to build up the system to the thermodynamic limit by successively increasing the size of the lattice in real space, creating an infinite system. This growth procedure is depicted in Fig. 2.1a. In each step, the lattice size is doubled by joining the Hamiltonian describing the lattice or "block" from the previous step to a copy of itself. The exponential growth of the matrices that must be diagonalised is controlled by keeping only the D lowest lying eigenstates of the Hamiltonian at each step and transforming all operators into this truncated basis.

One of the reasons that the NRG method is so successful when applied to impurity models is that the coupling between each of the layers in the discretized system gets exponentially smaller the farther from the impurity one gets [27, 30]. This is not true of the coupling between the blocks in a real space algorithm. It was thus expected that a real space calculation would give only qualitatively correct results. However, the lack in accuracy of this method was even worse than anticipated.

This approach fails because the low lying eigenstates of the two blocks joined together do not properly approximate the low lying eigenstates of the infinite system blocks. That is, the blocks will have different boundary conditions, at the ends where they join, to the whole system at the same point in the lattice [29]. Improvement in the accuracy of real space calculations is seen for a system consisting of a single-particle on a lattice when combinations of boundary conditions were applied in each step. However, when applied to a many-body chain, all combinations of boundary conditions for each single-particle wave function on each site of the chain need to be considered [30]. Unfortunately, this is too impractical to implement in practice.

The solution to this problem requires a different form of truncation as well as a

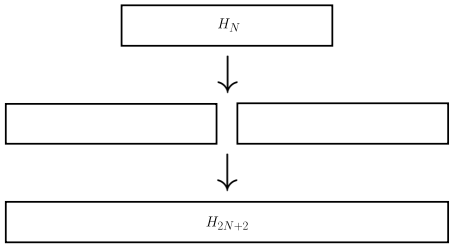

(a) The real space growth procedure consists of doubling the system size with each iteration. Two system blocks H_N are joined at each step to form H_{2N+2}. The ground state in the thermodynamic limit is approached by making the system sufficiently large.

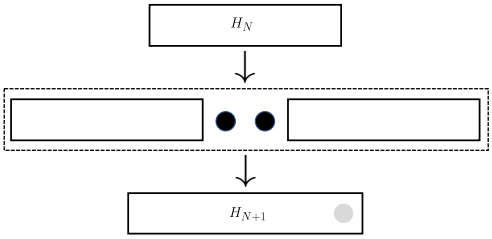

(b) The DMRG method simulates the thermodynamic limit by embedding the system in an environment. This is done by diagonalising the superblock depicted in the second row of the diagram. The system block H_N is grown by one site to form H_{N+1} in each iteration.

different way of building the blocks. This is the DMRG procedure. In the first step of DMRG, instead of growing the system by joining two blocks as in real space growth, a superblock is introduced. The superblock has $2N + 2$ sites and its Hamiltonian is formed from the Hamiltonian of a block with N sites. This is done by joining two copies of the N site block with two single sites between the two copies. In DMRG, sites 1 to$N$ of the superblock are viewed as an N site system block with a site added to it on site $N + 1$. Sites $N + 2$ to $2N$ of the superblock constitute an environment block with a site added to it. This allows for the simulation of the system in the thermodynamic limit by embedding it in its environment. Thus, the system grows by a single site in each step instead of it doubling. This growth procedure is illustrated in Fig 2.1b.

From this point, the Hamiltonian of the superblock is diagonalised and the ground state is obtained. This calculation can be implemented efficiently despite the large size of the Hilbert space because the superblock Hamiltonian is a sparse matrix and we only compute one eigenvector. Once the ground state of the superblock is obtained, the density matrix of the superblock is formed in preparation for the truncation procedure. The truncation method relies on the eigenvectors of the reduced density matrix of the system rather than on the system's low lying eigenstates. The environment is traced out of the superblock density matrix to form the reduced density matrix of the system block with a site added to it. Thus, the dimensions of the reduced density matrix are double the dimensions of the Hamiltonian for the N site system. This matrix is now diagonalised but only the

D eigenvectors with largest eigenvalues are kept. The Hamiltonian of the system with a site added to it is projected onto the subspace spanned by the truncated matrix of eigenvectors. This gives an approximate formulation of the $N+1$ site chain in a D-dimensional Hilbert space. We also project the spin operators from site $N+1$ so that we have everything we need to proceed to the $N+2$ site problem. From this point the process is repeated and so the system can be built up to the required size iteratively.

Conceptually, this algorithm is simple, however the implementation of it is non-trivial. Furthermore, it is not yet clear that there will be an improvement in accuracy of the DMRG procedure over the real space algorithm. Section 2.1 will motivate the truncation procedure further and thus show the validity of DMRG in approximating the Hilbert space of the system. In Section 2.2, explicit details of the implementation of the algorithm will be given. Moreover, the method that has been described is only the first stage of DMRG, known for historical reasons as infinite system DMRG. Once the system has been built up to the desired length, infinite system DMRG is followed by finite system DMRG. Finite system DMRG is very similar to infinite system DMRG but the superblock is built from left and right subsystems that are not identical. This is discussed further in Section 2.5. The following discussion of the truncation procedure is kept more general for this reason and it is not assumed that the system and environment are identical.

2.1 Truncation of the basis

The ground state of the superblock $|\psi\rangle$ can be expressed as the bipartite state

$$|\psi\rangle = \sum_{l,r} \psi_{l,r} |l\rangle |r\rangle , \tag{2.11}$$

where, l runs from one to L which is the number of states $|l\rangle$ in the left (system) block, r runs from 1 to R which is the number of states $|r\rangle$ in the right block and $\psi_{l,r}$ are the coefficients corresponding to each state. The state of the system, that is in contact with the environment, is expressed in the form of a reduced density matrix. This matrix is formed by tracing out the degrees of freedom of the environment from the density matrix of the superblock ground state. The matrix

elements of the reduced density matrix of the system are given by

$$\begin{aligned}\rho_{ll'} &= \langle l| \rho |l'\rangle \\ &= \sum_r \langle l, r|\psi\rangle \langle \psi|l', r\rangle \\ &= \sum_r \psi_{l,r}\psi^*_{l',r} \,. \end{aligned} \tag{2.12}$$

The orthonormal eigenstates of this matrix have positive eigenvalues w_j that sum to one. The matrix is then expressed in terms of these eigenstates $|w_j\rangle$ as

$$\rho |w_j\rangle = w_j |w_j\rangle \,. \tag{2.13}$$

Here, each eigenvalue represents the probability of the system to be in the corresponding eigenstate [30].

The density matrix is used in DMRG to find the best approximation of the ground state. The discussion given here on how this is done follows the original motivation by White done in 1993 [30]. To make the argument simpler, real coefficients are assumed for the wavefunctions and the superblock is assumed to be in a pure state. The argument can be extended for a mixed state and complex coefficients which yields a slightly different result for the accuracy of the chosen truncation but the motivation still holds. If $|\psi\rangle$ is the exact state of the superblock and $|\psi'\rangle$ is the approximate state formed after truncating the Hilbert space, then the best approximation will minimise the norm $|\,|\psi\rangle - |\psi'\rangle\,|^2$ [1]. The approximate wave function $|\psi'\rangle$ is expressed as

$$|\psi'\rangle = \sum_{r,j} a_{j,r} |u_j\rangle |r\rangle \,, \tag{2.14}$$

in terms of the states for the right block $|r\rangle$, the approximate system states $|u_j\rangle$ and the associated real coefficients $a_{j,r}$. The index r runs over 1 to R as before but j runs from 1 to the maximum number of allowed states in the final approximation, D. The orthonormal states $|u_j\rangle$ are given in terms of the states of the left block $|l\rangle$ as

$$|u_j\rangle = \sum_{j,l} u_{j,l} |l\rangle \,, \tag{2.15}$$

where, $|l\rangle$ are the states appearing in Eq. 2.11.

Using these definitions, the norm $|\,|\psi\rangle - |\psi'\rangle\,|^2$, is given by

$$\begin{aligned}
&\sum_{l,r}(\psi_{l,r} - \sum_j a_{j,r}\,|u_j\rangle\,|r\rangle)^2 \\
&= \sum_{l,r}(\psi_{l,r}^2 - 2\sum_j \psi_{l,r}a_{j,r}u_{j,l} + \sum_j a_{j,r}^2 u_{j,l}^2) \\
&= 1 - 2\sum_{l,r,j}\psi_{l,r}a_{j,r}u_{j,l} + \sum_{j,r} a_{r,j}^2. \qquad (2.16)
\end{aligned}$$

The last step follows from the orthonormality of the states. The last line is minimised [1] when $a_{j,r} = \sum_l \psi_{l,r}u_{j,l}$. Using this and the definition of the reduced density matrix $\rho_{ll'}$ gives

$$\begin{aligned}
&1 - 2\sum_{l,r,j}\psi_{l,r}a_{j,r}u_{j,l} + \sum_{r,j} a_{j,r}^2 \\
&= 1 - \sum_{l,l',r,j}\psi_{l,r}\psi_{l',r}u_{j,l'}u_{j,l} \\
&= 1 - \sum_{l,l',r,j} u_{j,l'}\psi_{l,r}\psi_{l',r}u_{j,l} \\
&= 1 - \sum_{l,j} u_{j,l'}\rho_{ll'}u_{j,l}. \qquad (2.17)
\end{aligned}$$

From the properties of the density matrix, this will be minimised when $u_{j,l}\,|j\rangle$ is an eigenstate of the density matrix with eigenvalue w_j. Thus, the norm becomes

$$|\,|\psi\rangle - |\psi'\rangle\,|^2 = 1 - \sum_j w_j. \qquad (2.18)$$

This shows that in order to choose the optimal truncation for the basis, the eigenstates with largest eigenvalues of the reduced density matrix of the system must be chosen. The quantity on the right hand side of Eq. 2.18 is called the truncated weight and it gives the error associated with the truncation as long as the system is embedded in the final environment and that environment is exactly described. This is not usually the case because the superblock Hamiltonians are built iteratively and in each step an approximate representation of the blocks is used. Thus, in each step we have neither the final environment nor an exact

representation. Therefore, this quantity gives a lower bound on the true error made in the approximation using this truncation method.

From this argument it is clear that, for a system to be approximated well by only a few states, the eigenvalues must decrease quickly so that the sum of the kept eigenvalues is close to one. This condition, for which systems will be well described using DMRG, is made more concrete using the entanglement entropy of the system in the environment. The entanglement entropy is given in terms of the reduced density matrix of the system as $\mathrm{Tr}\rho\log\rho$ [4]. The truncation using the eigenvectors with the highest eigenvalue ensures that as much entanglement between the system and environment is kept as possible.

The systems that are described best by DMRG are then the ones where the entanglement entropy grows slower than the system size. In fact, gapped systems with local interactions (like the Heisenberg chain studied here) have an entanglement entropy that scales with an area law. This means that for a one-dimensional system like the one studied, the entanglement entropy is a constant and so it does not increase with the system size. Therefore, the states are well approximated when they are truncated to a sufficiently large D that will however, remain constant as we increase system size N. In Section 2.2, the implementation of the DMRG algorithm using this truncation is detailed. Systems with states that obey this area law can be efficiently parametrised using the matrix product state formalism. This allows one to formulate DMRG as a variational calculation that minimises the expectation value of the ground state energy.

2.2 DMRG implementation for the Heisenberg chain

Each iteration in the infinite system DMRG method follows the following steps:

(i) The Hamiltonian and spin operators from the previous step are used to create H_{N+1} the Hamiltonian of a system that is one site bigger.

(ii) Two copies of H_{N+1} are then joined to form a superblock Hamiltonian.

(iii) The ground state of the superblock is determined by diagonalising the superblock Hamiltonian.

(iv) The ground state is then used to form the density matrix of the combined system and environment.

(v) The reduced density matrix is then formed by tracing out the environment degrees of freedom.

(vi) This matrix is now diagonalised and the D eigenvectors with largest eigenvalues are kept and form the new basis.

(vii) The operators and Hamiltonian for the system of size $N+1$ are now transformed to this new basis and in the process they will be truncated.

How each of these steps was implemented is explored in more detail in the next sections.

2.2.1 Adding a site to the existing chain and building the superblock

The growth of the chain through the iterative addition of sites has already been discussed. In the language of DMRG, the existing chain is known as the system block and in each step a site is added to this block. For the very first step, the system block will contain one site and by adding a site, the two site Hamiltonian in Eq. 2.3 is reached. In practice, the step in the algorithm that will add a site is started by adding the matrix H_N on the diagonals of the new matrix. This is equivalent to the Kronecker product with the 2×2 identity matrix and is given by the matrix H_{block},

$$H_{\text{block}} = \begin{pmatrix} H_N & 0 \\ 0 & H_N \end{pmatrix}, \tag{2.19}$$

which has the matrix H_N on the diagonals. This is then added to the tensor product involving the spin matrices given in Eq. 2.9. This gives the matrix H_{N+1} indexed by A and B

$$H_{N+1_{A,B}} = H_{\text{block}} + \sum_{i \in \{x,y,z\}} J_i S^i_{N_{\alpha\beta}} \sigma_{a,b}, \tag{2.20}$$

where, the index A is related to α, a and the number of rows, L, of the left block matrix before the addition of the site by

$$A = \alpha + L(a-1). \tag{2.21}$$

The relationship between B, β and b follows similarly.

The system must now be embedded in an environment that resembles the thermodynamic limit. This is achieved by creating the superblock Hamiltonian which is formed by joining the system block to the environment block, which is its mirror image as represented in Fig. 2.1b. This array can be given in terms of its elements in the same way as for adding a site to the block. That is,

$$\begin{aligned} H_{(\alpha_1 a_1 \beta_1 b_1),(\alpha_2 a_2 \beta_2 b_2)} =& H^{N+1}_{(\alpha_1 a_1),(\alpha_2 a_2)} \delta_{\beta_1 \beta_2} \delta_{b_1 b_2} + H^{N+1}_{(\beta_1 b_1),(\beta_2 b_2)} \delta_{\alpha_1 \alpha_2} \delta_{a_1 a_2} \\ &+ \sum_{i \in \{x,y,z\}} J_i \sigma^i_{a_1 a_2} \sigma^i_{b_1 b_2} \delta_{\alpha_1 \alpha_2} \delta_{\beta_1 \beta_2}. \end{aligned} \tag{2.22}$$

The superblock is most easily represented as an array with eight indices because the indices of the system block with a site added $\alpha_1, a_1, \beta_1, b_1$ and the environment block with a site added $\alpha_2, a_2, \beta_2, b_2$ can all be used in the representation. This array could be formed into a matrix in a similar way to adding a site to the block. Once the superblock matrix is formed, it can be numerically diagonalised and the ground state of the system embedded in an environment can be found. However, explicitly building, storing and then diagonalising the matrix is computationally expensive. As its turns out this is ultimately unnecessary and this is discussed in the next section.

2.2.2 Diagonalising the superblock

When diagonalising the superblock the only result which is required is the state which is targetted, which is the ground state. For this reason and because the matrix has a block diagonal form, it is possible to solve for this state quite efficiently using the Lanczos algorithm [31]. This algorithm starts with a randomly generated vector and iteratively improves the approximation of this vector to a specified eigenvector of the matrix of interest.

The Lanczos algorithm used in this work was performed using the ARPACK-NG package. The smallest eigenvalue and its associated eigenvector is calculated. This must be done in a way that avoids splitting degeneracies and so if the ground state of the spin chain is sought after, the first two eigenvectors of the superblock matrix are found in practice. This is because this system is expected to have a twofold degeneracy in the ground state. The tolerance of the algorithm was set to 10^{-16} and so the maximum accuracy it can give is 16 significant digits or double precision. This is chosen so that the error in the diagonalisation does not exceed the error of the truncation.

It is more efficient to build this product using the definition of the elements of the Hamiltonian given in Eq. 2.22 than it would be to explicitly build the whole Hamiltonian in matrix form and then perform the product. This is because the matrix is structured in the block diagonal way mentioned already. For each step, the Hamiltonians for each block as well as the block operators and the Pauli matrices are all that must be stored. The result of the matrix vector product is calculated as a four dimensional array $v_{\alpha a \beta b}$ which is shaped into a vector for use in the Lanczos algorithm. The product is given by the operation

$$\sum_{\alpha' a' \beta' b'} H_{(\alpha a \beta b),(\alpha' a' \beta' b')} u_{\alpha' a' \beta' b'} = v_{\alpha a \beta b}, \tag{2.23}$$

where, $u_{\alpha' a' \beta' b'}$ is the vector that is input by the Lanczos algorithm. In general, the computer will have to do $L \times R \times 4$ multiplications and additions to compute each element of the vector. Thus, to compute the entire vector will take of the order $L^2 \times R^2$ operations. However, the result of many of the multiplications is zero because the Hamiltonian is sparse. The non-zero elements are given by

$$\begin{aligned} v_{\alpha a \beta b} = & \sum_{\alpha'} H_{N_{\alpha\alpha'}} u_{\alpha' a \beta b} + \sum_{\beta'} H_{N_{\beta\beta'}} u_{\alpha a \beta' b} \\ & + \sum_{i \in \{x,y,z\}} J_i \Big[\sum_{\alpha'} S^i_{N_{\alpha\alpha'}} \sum_{a'} \sigma^i_{aa'} u_{\alpha' a' \beta b} \\ & + \sum_{\beta'} S^i_{N_{\beta\beta'}} \sum_{b'} \sigma^i_{bb'} u_{\alpha a \beta' b'} \\ & + \sum_{b'}^{i} \sigma^i_{bb'} \sum_{a'} \sigma^i_{aa'} u_{\alpha a' \beta b'} \Big], \end{aligned} \tag{2.24}$$

where, $H_{N_{\alpha\alpha'}}$ and $S^i_{N_{\alpha\alpha'}}$ are the Hamiltonian and spin operators for the left block that are formed at the end of the previous iteration and the operators indexed by β and β' are for the right block. Thus, the computation of each element takes at most L or R operations. The computation time of the matrix elements is thus of the order $L^2R + R^2L$.

Thus, in each DMRG iteration the superblock is not built, but rather, the operators from the previous step are input into a diagonalising subroutine which performs the required product. Once the final iteration is reached and the superblock is the desired size, the ground state calculated in this step is used for any further calculations of observables.

2.2.3 Creating the reduced density matrix of the system

Once the ground state of the superblock has been found, the Hilbert space must be truncated using the reduced density matrix. The ground state is a vector that must be reshaped into a matrix in order to calculate the reduced density matrix. When the ground state is expressed as in Eq. 2.11, the coefficients $\psi_{l,r}$ are the entries in the vector. The vector has $4LR$ entries where L and R are the dimensions of the number of rows or columns of the left and right block Hamiltonians before the addition of a site. The vector entries are arranged into the matrix Ψ which is $2L \times 2R$ in size. The reduced density matrix for the left block with a site added to it is then by definition

$$\rho_{ll'} = \sum_r \psi_{l,r}\psi_{l',r}, \tag{2.25}$$

where, r runs from 1 to $2R$. This is equivalent to the product $\rho_{ll'} = \Psi\Psi^T$, where T denotes the transpose. For the right block it would be $\rho_{rr'} = \Psi^T\Psi$, or

$$\rho_{r,r'} = \sum_l \psi_{l,r}\psi_{l,r'}, \tag{2.26}$$

where, l runs from 1 to $2L$. Once formed, the reduced density matrix of the left block is then diagonalized, the eigenvectors are sorted by the size of their eigenvalues and the D eigenvectors with highest eigenvalues are kept in matrix C which is $2L \times D$ in size. At this stage it is only necessary to do this for the left block because the system and its environment, which corresponds to the right

block, are the same. The truncated weight which represents a maximum accuracy that can be achieved can also be calculated at this point using Eq. 2.18.

2.2.4 Truncating the operators using the new basis

The matrix C, consisting of the truncated eigenvectors of the system's reduced density matrix, can now be used to truncate the operators for the system with a site added. To do this, first the Hamiltonian for the block with a site added must be formed. This is done according to Eq. 2.10. That is, starting from the Hamiltonian H_N, the Hamiltonian H_{N+1} which is twice as big has been formed. Then, the truncated operator for the bigger system H'_{N+1}, is expressed in the new truncated basis by the transformation

$$H'_{N+1} = C^T H_{N+1} C. \tag{2.27}$$

Similarly, the spin operators for the block with an added site must also be built using Eq. 2.9. These operators are then transformed in the same way as the Hamiltonian.

2.3 Exact Diagonalization of the Hamiltonian with no interactions

The results of the DMRG program that are used to study the Heisenberg chain are checked against an exact solution of the model in the absence of interactions. For ease of reference, the non-interacting part of the Hamiltonian that was given in the introduction is repeated here, with a modification to the order parameter because the system has no junction. The junction requires very little modification to the calculation and this is outlined at the end of the section. The Hamiltonian,

$$H_{2N_0} = -\frac{W}{2}\sum_{j=1}^{2N-1}(a_j^\dagger a_{j+1} + a_{j+1}^\dagger a_j) - \frac{\Delta}{2}\sum_{j=1}^{2N-1}(a_j a_{j+1} + a_{j+1}^\dagger a_j^\dagger), \tag{2.28}$$

is quadratic in fermionic creation and annihilation operators and so it can be described using a Bogoliubov de Gennes Hamiltonian [6]. In order to do this, it is

written in matrix form

$$H = \frac{1}{2}\sum_{m,n=1}^{N} A_{mn}a_m^\dagger a_n + A_{mn}a_n^\dagger a_m + B_{mn}a_m^\dagger a_n^\dagger + B_{mn}a_n a_m, \tag{2.29}$$

where, A_{mn} and B_{mn} are elements of the matrices

$$A = -\frac{W}{2}\begin{pmatrix} 0 & 1 & 0 & 0 & 0 & \cdots \\ 1 & 0 & 1 & 0 & 0 & \cdots \\ 0 & 1 & 0 & 1 & 0 & \cdots \\ \vdots & & & & & \end{pmatrix}, \quad B = -\frac{\Delta}{2}\begin{pmatrix} 0 & 1 & 0 & 0 & 0 & \cdots \\ -1 & 0 & 1 & 0 & 0 & \cdots \\ 0 & -1 & 0 & 1 & 0 & \cdots \\ \vdots & & & & & \end{pmatrix}. \tag{2.30}$$

Matrix B is antisymmetric because of the anti-commutation relation between the fermions. Eq. 2.29 is rearranged so that the index m is on the left and n is on the right. This yields

$$\begin{aligned} H_{N_0} =& \frac{1}{2}\sum_{m,n=1}^{N} A_{mn}a_m^\dagger a_n + B_{mn}a_m^\dagger a_n^\dagger - B_{mn}a_m a_n - \frac{1}{2}\sum_{m\neq n}^{N} A_{mn}a_m a_n^\dagger \\ &+ \frac{1}{2}\sum_{n=1}^{N} A_{nn}(1 - a_n a_n^\dagger) \\ =& \frac{1}{2}\sum_{m,n=1}^{N} A_{mn}a_m^\dagger a_n + B_{mn}a_m^\dagger a_n^\dagger - B_{mn}a_m a_n - A_{mn}a_m a_n^\dagger + \frac{1}{2}\mathrm{Tr}A, \end{aligned}$$

which, with

$$\begin{pmatrix} \mathbf{a}^\dagger & \mathbf{a} \end{pmatrix} = \begin{pmatrix} a_1^\dagger & \cdots & a_N^\dagger & a_1 & \cdots & a_N \end{pmatrix},$$

can be represented in matrix form as

$$H_{N_0} = \frac{1}{2}\begin{pmatrix} \mathbf{a}^\dagger & \mathbf{a} \end{pmatrix}\begin{pmatrix} A & B \\ -B & -A \end{pmatrix}\begin{pmatrix} \mathbf{a} \\ \mathbf{a}^\dagger \end{pmatrix} + \frac{1}{2}\mathrm{Tr}A. \tag{2.31}$$

The matrix,

$$H_{\mathrm{BdG}} = \begin{pmatrix} A & B \\ -B & -A \end{pmatrix},$$

is the Bogoliubov de Gennes Hamiltonian. Its eigenvectors come in pairs with positive and negative eigenvalues. Let $\binom{x}{y}$ be an eigenvector of H_{BdG} with eigenvalue λ. Then, consider the application of H_{BdG} to the vector$\binom{y}{x}$. The

result of this is

$$\begin{aligned} Ay + Bx &= (Ay + Bx) \\ &= -(-Bx - Ay) \\ &= -\lambda y \qquad (2.32) \\ -Ax - By &= -(Ax + By) \\ &= -\lambda x. \qquad (2.33) \end{aligned}$$

Therefore, $\binom{y}{x}$ is also an eigenvector of H_{BdG} with eigenvalue $-\lambda$. The matrix containing the normalised eigenvectors of H_{BdG} then has the structure

$$\begin{pmatrix} U & V \\ V & U \end{pmatrix}, \qquad (2.34)$$

where, the first N columns correspond to eigenvectors with positive eigenvalues and the last N correspond to those with negative eigenvalues. Since H_{BdG} is real, so too are U and V. Then because this is the matrix of normalised eigenvectors we must have that

$$\mathbb{1}_{N\times N} = \begin{pmatrix} U & V \\ V & U \end{pmatrix} \begin{pmatrix} U & V \\ V & U \end{pmatrix}^{\mathrm{T}}, \qquad (2.35)$$

where, T denotes the transpose. In component form, this is

$$\begin{aligned} \sum_{k=1}^{N} (u_{km}u_{kn} + v_{km}v_{kn}) &= \delta_{m,n} \qquad (2.36) \\ \sum_{k=1}^{N} (u_{km}v_{kn} + v_{km}u_{kn}) &= 0. \end{aligned}$$

Bogoliubov operators are now defined that are a linear superposition of creation and annihilation operators. These operators are defined as

$$d_m = \sum_{k=1}^{N} u_{km}a_k + v_{km}a_k^\dagger \quad \text{and} \quad d_m^\dagger = \sum_{k=1}^{N} u_{km}a_k^\dagger + v_{km}a_k \qquad (2.37)$$

and are fermionic. That is, they satisfy

$$\{d_k, d_l\} = 0 \quad \text{and} \quad \{d_k^\dagger, d_l\} = \delta_{k,l}. \qquad (2.38)$$

The proof of this relies on the structure of H_{BdG} and is detailed in Appendix B. H is then diagonalized by these new operators

$$\begin{aligned} H_{N_0} =& \frac{1}{2}\begin{pmatrix}\mathbf{a}^\dagger & \mathbf{a}\end{pmatrix}\begin{pmatrix} A & B \\ -B & -A\end{pmatrix}\begin{pmatrix}\mathbf{a} \\ \mathbf{a}^\dagger\end{pmatrix} + \frac{1}{2}\mathrm{Tr}A \\ =& \frac{1}{2}\begin{pmatrix}\mathbf{d}^\dagger & \mathbf{d}\end{pmatrix}\begin{pmatrix} U & V \\ V & U\end{pmatrix}\begin{pmatrix} E & 0 \\ 0 & -E\end{pmatrix}\begin{pmatrix} U & V \\ V & U\end{pmatrix}\begin{pmatrix}\mathbf{d} \\ \mathbf{d}^\dagger\end{pmatrix} + \frac{1}{2}\mathrm{Tr}A. \end{aligned} \tag{2.39}$$

Here, E is a diagonal matrix with $E_{nn} = E_n$ the nth element on the diagonal.

The Hamiltonian in component form is then

$$\begin{aligned} H_{N_0} =& \frac{1}{2}\sum_{k=1}^{N}(E_k d_k^\dagger d_k - E_k d_k d_k^\dagger) + \frac{1}{2}\mathrm{Tr}A \\ =& \frac{1}{2}\sum_{k}(E_k d_k^\dagger d_k - E_k(1 - d_k^\dagger d_k) + \frac{1}{2}\mathrm{Tr}A \\ =& \frac{1}{2}\sum_{k} E_k d_k^\dagger d_k - \frac{1}{2}\mathrm{Tr}E + \frac{1}{2}\mathrm{Tr}A. \end{aligned} \tag{2.40}$$

The ground state $|GS\rangle$ has energy $1/2\ \mathrm{Tr}A - 1/2\ \mathrm{Tr}E$, since $d_k\,|GS\rangle = 0$. Thus, in order to get the exact ground state energy of the N site system, all that remains to be done is to diagonalize H_{BdG} numerically. Later in the dissertation, the exact solution for the non-interacting system, where the order parameter has different signs on opposite sides of a junction, is required. The method used in this subsection is sufficient for this. However, matrix B must be modified in H_{BdG} to reflect the addition of the junction. It is then

$$B = -\frac{\Delta}{2}\begin{pmatrix} 0 & 1 & 0 & 0 & \cdots & & & & \\ -1 & 0 & 1 & 0 & \cdots & & & & \\ 0 & -1 & 0 & 1 & \cdots & & & & \\ & & & & \vdots & & & & \\ & & & \cdots & 0 & \cdots & & & \\ & & & & \vdots & & & & \\ & & & & \cdots & 1 & 0 & -1 & 0 \\ & & & & \cdots & 0 & 1 & 0 & -1 \\ & & & & \cdots & 0 & 0 & 1 & 0 \end{pmatrix}, \tag{2.41}$$

where, the Nth row is zero corresponding to the site with the junction and the sign of Δ changes from site $N+1$.

2.3.1 Performance of the DMRG code

The infinite system DMRG program was used to build an 82 site chain without a junction. The values chosen for the couplings were $\{W, \Delta, U\} = \{1.0, -0.2, 0\}$. The three lowest energies that are obtained form diagonalising the 82 site superblock are compared to the exact solution of the non-interacting Hamiltonian of the system. These three energies correspond to the degenerate ground state and the first state in the band. The results for the exact energy E_{Exact} and the energy calculated from DMRG, E_{DMRG}, are shown in Fig. 2.2 as a function of how many states D are kept during truncation. The yellow line represents the first energy in the band, the blue and the red represent the degenerate ground state. The red line is the state with the smallest energy and so it is the one that is targetted by the infinite system DMRG program.

The accuracy of the ground state converges to 13 significant digits when 64 states are kept and there are 12 significant digits when 56 states are kept. The truncated weight given by Eq. 2.18 was of the order of 10^{-11} for 56 kept states and so the accuracy of the calculation is the same as the minimum error that is associated with the truncation. The time it takes to perform the calculation is proportional to D^3. Thus, an acceptable accuracy needs to be chosen while taking into account the computational time. There is a much lower accuracy achieved for the states in the band. This is addressed in Sec. 2.6 when a modification of the method to calculate low lying excited states is discussed.

2.4 The effect of building the system in a different environment

The infinite system DMRG program performs well for the spin chain that was considered. This was expected as similar performance was achieved in the initial studies done to test the DMRG method in the 1990's which were also done with spin chains [32]. In Chapter 3, we will study interactions in a chain with a Josephson

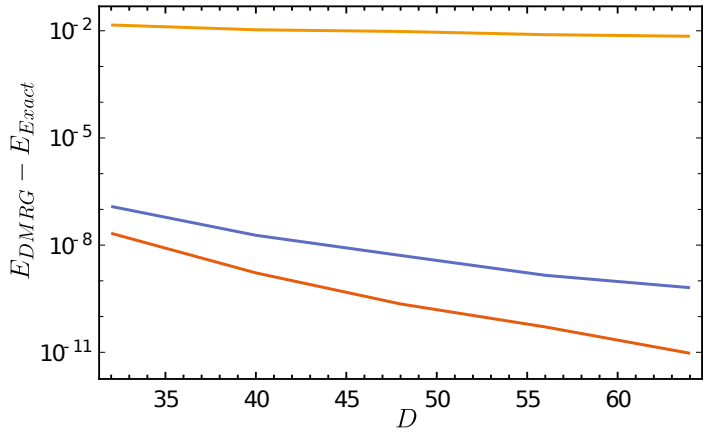

Figure 2.2: The difference from the exact energies of the infinite system DMRG algorithm decreases for an increasing number of kept states D. Here, $\{W, \Delta, U\} = \{1.0, -0.2, 0\}$, the chain has 82 sites and there is no junction. The yellow line represents the difference in value between the first state in the band obtained from the DMRG program and the exact energy calculated. The red line represents the difference for the ground state and the blue line represents the difference for the second energy in the spectrum which should be degenerate with the ground state.

Junction. In particular, the case where the sign of the order parameter changes at the junction will be of interest. In the superblock Hamiltonian, this corresponds to swapping the couplings J_x and J_y in the environment block compared to the system block. Using infinite system DMRG, the accuracy of this approach where the environment is no longer identical to the system is tested.

The matrix vector product used to diagonalise the superblock with different system and environment blocks is

$$\begin{aligned} v_{\alpha a \beta b} = &\sum_{\alpha'} H_{N_{\alpha\alpha'}} u_{\alpha' a \beta b} + \sum_{\beta'} H_{N_{\beta\beta'}} u_{\alpha a \beta' b} \\ &+ \sum_{i \in \{x,y,z\}} \Big[J_i^{\text{left}} \sum_{\alpha'} S^i_{N_{\alpha\alpha'}} \sum_{a'} \sigma^i_{aa'} u_{\alpha' a' \beta b} \\ &+ \sum_{\beta'} J_i^{\text{right}} S^i_{N_{\beta\beta'}} \sum_{b'} \sigma^i_{bb'} u_{\alpha a \beta' b'} \\ &+ \sum_{b'} J_i^{\text{junction}} \sigma^i_{bb'} \sum_{a'} \sigma^i_{aa'} u_{\alpha a' \beta b'} \Big], \end{aligned} \tag{2.42}$$

where, J_i^{left}, J_i^{right} and J_i^{junction} are the couplings on the left, right and at the junction.

In terms of the fermionic couplings discussed before, the Josephson junction is produced by setting W the same throughout the superblock but making the order parameter Δ positive on one side and negative on the other. We chose $\{W, \Delta, U\} = \{1.0, -0.2, 0\}$ for the system (left) block and $\{W, \Delta, U\} = \{1.0, 0.2, 0\}$ for the environment or right block. The couplings between the system and environment were set to be $\{W, \Delta, U\} = \{1.0, 0, 0\}$.

Once again, an 82 site chain was built and this time, the first five energies were calculated. These are depicted in Fig. 2.3 as a difference between the exact value for the energy and the value calculated from DMRG. The green line represents the first energy in the band. The four lines below this represent the fourfold degenerate ground state. Again the change in accuracy is given with respect to the number of states that are kept. The figure shows that after the addition of the junction,

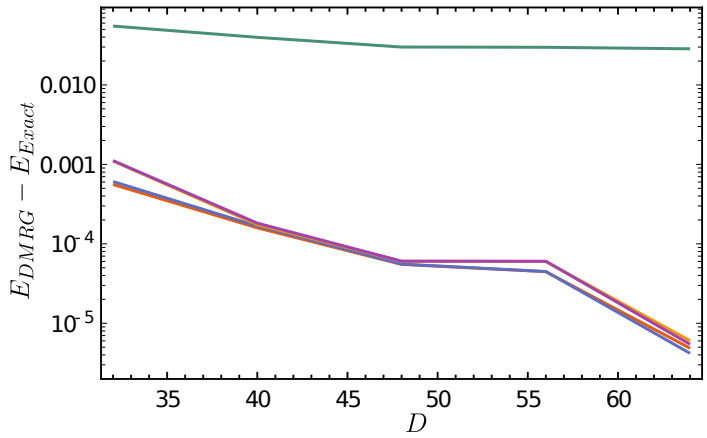

Figure 2.3: The difference from the exact energies of the infinite system DMRG algorithm decreases for an increasing number of kept states D. Here, $\{W, |\Delta|, U\} = \{1.0, 0.2, 0\}$, the chain has 82 sites and there is a Josephson junction with a different sign for the order parameter on each side. At the junction, $\{W, \Delta, U\} = \{1.0, 0, 0\}$. The green line depicts the difference in value between the energy calculated for the first state in the band using DMRG and the exact state. The same difference for the fourfold degenerate ground state energies are represented by the red, blue, orange and purple lines.

the convergence to the exact states is much worse, with the ground state only reaching seven significant digits for the maximum number of kept states. However, the truncated weight is still is of the order 10^{-11}.

Building the block with a Josephson junction in the middle with a π phase

difference between each side means that the left block is no longer a mirror image of the right block. The reduced density matrix for the left and right blocks must both be calculated and used to truncate the operators for the left and right blocks, respectively. However, a lower accuracy in the ground state energy is expected. This is because in the first few DMRG steps the environment and system blocks are small. Thus, most sites in the system block are close to the junction with the environment. This is not the case as the chains on either side grow and so the initial steps do not simulate the final system embedded in an environment well [1]. The accuracy of the ground state can be improved by implementing finite system DMRG. This modification of the program is elaborated on in the next section.

2.5 Finite system DMRG

Once a system of a suitable size has been built using infinite system DMRG, the accuracy of the calculation of the ground state can be greatly improved using finite system DMRG. Finite system DMRG performs very similar steps to infinite system DMRG. At the end of the final iteration of infinite system DMRG, a superblock with $2N + 2$ sites is built with a left block and right block of equal length N and two additional sites joining the two blocks. The finite system algorithm does not change the number of sites in each block, instead the superblock of $2N + 2$ sites is built but the left and right blocks will have different lengths. For this to be possible, the operators for each step of infinite system DMRG for the left and right of the superblock must be saved.

Finite system DMRG proceeds as follows. In the first iteration, the left block operators from the last step of the infinite algorithm are used to build a $N + 1$ site chain. Additionally, the right block operators from the second last step are retrieved from storage. These are used to build a right block with N sites by adding a site to the retrieved operators for the $N - 1$ site chain. Once the superblock is built, the algorithm continues in the same way as before. The reduced density matrix of the left block with a site added is formed from the ground state of the superblock as described in Sec. 2.2.3. The D eigenvectors of this matrix with largest eigenvalues are used to project the operators of the $N + 2$ site chain onto the truncated basis as described in Sec. 2.2.4. These operators are now also saved.

This process of growing the left block at the expense of the right block is repeated and all the operators are saved for the left block. In each step we are reducing the size of the right block.

Since it is not possible to deduce the matrices representing operators for a smaller block from those of a larger block, we approximate the smaller blocks as those that we encountered immediately before the current sweep. For instance, in the first sweep left, we use the stored right block operators we computed in infinite system DMRG, in the opposite order to that in which they were calculated. The final step will have a right block with a single site and a left block with $2N-3$ sites joined together by two single sites.

From this point, the entire process is reversed. The right block grows and its operators are updated and saved at the end of each step. For the left block, we use retrieved operators. Once the left block consists of a single site the left block is allowed to grow and all the updated left block operators are saved, up to the point when the left and right blocks are the same size. At this point, a full finite system 'sweep' has been performed. It was found in the initial work done in developing the DMRG method that for $S = 1$ and $S = 1/2$ Heisenberg chains, one to three sweeps are needed to improve the approximation enough to achieve an error that is almost the same as the truncated weight [30].

In general the couplings between the sites can be position dependent. The initial building of the chain in infinite system DMRG always has the junction between the system and environment blocks. However, when sweeping the junction is in the middle of the chain which may not be between the left and right blocks. This is illustrated in Fig 2.4. In the case with the junction the coupling J_i^j, for $i \in \{x, y, z\}$ and j the index of the site, will have the same values up to the point where $j = N$. These are all the sites to the left of the junction. The values J_i^{N+1} between $N+1$ and $N+2$ will be the coupling at the junction where $J_x = J_y$. The couplings to the right of the junction will be the same as the left with J_x and J_y reversed. The matrix vector product used to diagonalise the superblock Hamiltonian with a Junction is given by Eq 2.42 where, for finite system DMRG, J_i^{left}, J_i^{right} and J_i^{centre} are the couplings on the end of the left block, right block and between the two sites. When sweeping was incorporated into the existing

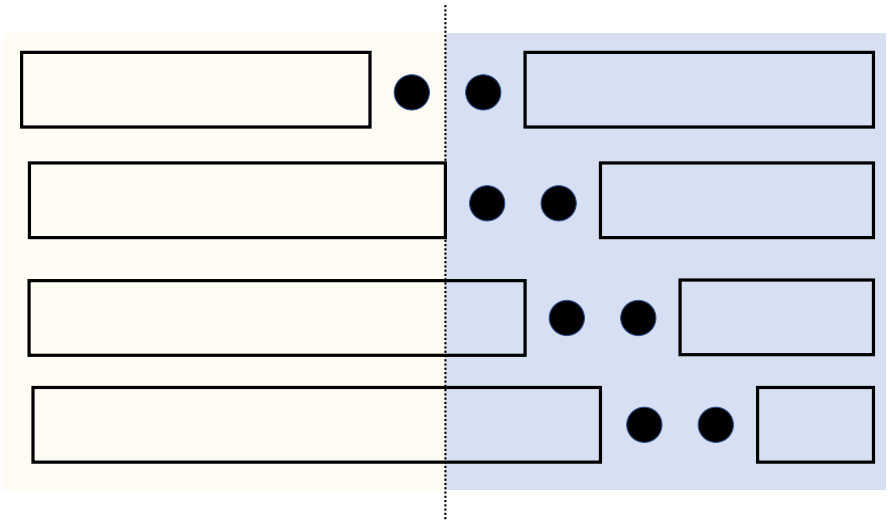

Figure 2.4: This diagram illustrates part of a sweep to the right during finite system DMRG. Initially, the superblock is built up with the junction in the middle using infinite system DMRG. The two sides of the junction have a π phase difference between them. This amounts to swapping the sign of Δ in the part of the chain that is shaded blue compared to the part that is shaded yellow. Once the system is built in this way sweeping begins. The diagram shows that as a sweep is performed, the choice of the parameters on either side of the joining of the superblock must change.

DMRG program, the ground state of the chain with a junction converges to the exact calculation to eight significant figures in the first sweep and no improvement is seen in subsequent sweeps.

Finite system DMRG can be formulated using matrix product states as a variational calculation. The matrix product state algorithm is essentially the same as finite system DMRG but a single site is added between left and right blocks instead of two sites [4]. The matrix product state formulation shows that the method is not purely heuristic. In this formulation, every step of finite system DMRG reduces the expectation value of the energy. A detailed review of the implementation of this method can be found in [4].

2.6 Calculation of excited states

DMRG is only optimal as an algorithm to find the ground state but the excited states of a system may also be of interest. The DMRG algorithm can be modified in a very simple way to achieve reasonable accuracy for the low lying excited states.

The only change that must be made is that once the superblock is diagonalized, the excited state of interest is used to form the reduced density matrix and this is then used to form the new basis for the system. In this way, it was found that for an $S = 1/2$ Heisenberg chain about fifteen states could be targetted with an acceptable accuracy [30].

When applying this method, it is possible that the algorithm will lose numerical stability. To correct for this, it is common practice to take a weighted average over the density matrices of all states from the ground state to the targetted state. The weighting in the average is usually taken to be equal for all the states in the summation. That is, for T the number of targetted states and ρ_i the reduced density matrix of the system for state i,

$$\rho_{average} = \frac{1}{T} \sum_{i=1}^{T} \rho_i. \tag{2.43}$$

To maintain accuracy, the number of kept states needs to increase with the number of targetted states. Therefore, this approach comes at the cost of computational time and accuracy especially when a large number of excited states need to be calculated [33].

The increase in accuracy for the algorithm with state averaging and targetting as well as for targetting with no average are shown in Fig. 2.5. The system has a junction present and two finite system sweeps were performed. The results for only the first state in the band are depicted here. The difference from the exact energy is shown as a function of an increasing number of kept states. The red line shows the behaviour of the calculation when the ground state is targetted as in standard DMRG. The blue line shows what happens when the first state in the band is targetted but no state averaging is applied. The yellow line shows how the algorithm performs when the first state in the band is targetted and a state average is included in the density matrix calculation. The results of these calculations show that the state averaging stabilises the algorithm so that the accuracy increases monotonically with an increased number of kept states. The figure shows that the first state in the band can be obtained accurately to six

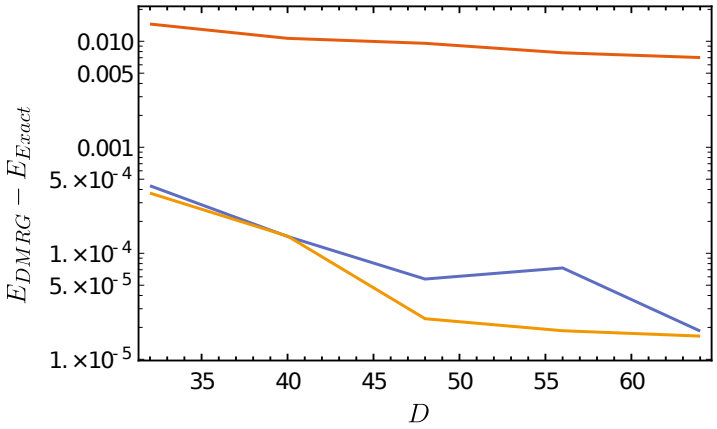

Figure 2.5: The accuracy of the calculation for the first state in the band is shown with respect to the number of kept states and the method of targetting. For this calculation, $\{W, |\Delta|, U\} = \{1.0, 0.2, 0\}$, the chain has 82 sites and there is a Josephson junction with a π phase difference between the two sides. At the Junction, $\{W, \Delta, U\} = \{1.0, 0, 0\}$. The red line shows the behaviour of the system when the band is not targetted, the blue line represents the behaviour when the first energy in the band is calculated but no state averaging is used and finally, the yellow line represents the performance of the DMRG calculation when the first state in the band is targetted and the state averaging method is applied.

significant digits if 56 states are kept, the state is targetted and a state average is included.

3 Zero-energy quasiparticles in an interacting nanowire containing a topological Josephson junction

The DMRG program that has been discussed in Chapter 2 is applied to a physically relevant system in this chapter. The system we consider is a one-dimensional nanowire with strong spin-orbit coupling that is in contact with a bulk s-wave superconductor. For the correct choice of system parameters, the wire hosts effectively spinless electrons. Thus, the pairing induced by the bulk superconductor is p-wave like. That is, the order parameter has negative spatial parity. The behaviour of most superconducting systems can be described using an effective single-particle description with Bogoliubov quasiparticles. This approach was used to solve the non-interacting system that was used to benchmark the algorithm in Chapter 2. However, the electrons in the one-dimensional wire interact with each other intrinsically via a Coulomb interaction. In the bulk superconductor, these interactions are screened and so the single-particle approach approximates the system well. However, in the wire, the bulk superconductor may not screen the interactions as well [7]. In one dimension, a mean field theory approach may not describe the intrinsic interactions well. Thus, in order to study the interactions, the full many-body system must be considered. This is done numerically in this work using DMRG.

An infinite spinless p-wave wire that hosts a Josephson junction hosts an unusual

Josephson effect. Usually, if the phase over a Josephson junction is changed adiabatically by 2π the system will return to its initial state because the spectrum is 2π periodic in the phase difference. Additionally, there are no level crossings and so as the phase is changed, the system remains in the ground state. Thus, the current through the junction is 2π periodic as a function of the phase across the junction. This is known as the 2π Josephson effect.

In Contrast to this, as the phase is adiabatically swept through 2π, the spinless p-wave wire the we consider will always have an odd number of level crossings between the ground state and the first excited state. This is as a result of the topologically non-trivial nature of the wire [34]. After the phase has been swept through 2π the system initially in the ground state is taken to the first excited state and it only returns to the ground state after a further sweep of 2π. This doubling in the periodicity of the current has been recently observed experimentally [35] and is called the 4π Josephson effect.

When the wires to the left and right of the junction are identical, the energy spectrum of the system is symmetric about the the phase difference π and hence, one of the level crossings happens at this point. We study the system at this value of the phase difference. If the electrons in the wire have no intrinsic interactions between them, the full energy spectrum is four-fold degenerate up to exponentially vanishing finite size corrections. In this chapter, using DMRG, we confirm that the four-fold degeneracy of the ground state is robust to particle-hole symmetric interactions provided the interactions are not too strong. This is consistent with the fact that the ground state degeneracy is topologically protected [34]. We also investigate whether the four-fold degeneracy of the excited states is also robust to the addition of these interactions. We find that this is indeed the case and deduce that interactions are not a source of quasiparticle poisoning of the 4π Josephson effect. That is, this effect will still be observed even if the system is initialised in a state with a few bulk quasiparticles rather than in the true ground state. Finally, the behaviour of finite size corrections is studied. In general, finite size corrections decay as a function of system size but they may still be observable in realistic systems [36]. We investigate how interactions affect these corrections.

However, before this analysis is performed, the Majorana operators for the non-

interacting system will be discussed so that the MZMs may be better understood. Interactions will then be added to the system and the main results of the work will be discussed. The non-interacting part of the Hamiltonian is given by

$$\begin{aligned} H_{2N_0} = &- \frac{W}{2}\sum_{j=1}^{2N-1}(a_j^\dagger a_{j+1} + a_{j+1}^\dagger a_j) \\ &+ \frac{\Delta}{2}\sum_{j=1}^{N-1}(a_j a_{j+1} + a_{j+1}^\dagger a_j^\dagger) \\ &- \frac{\Delta}{2}\sum_{j=N+1}^{2N-1}(a_j a_{j+1} + a_{j+1}^\dagger a_j^\dagger) \end{aligned} \tag{3.1}$$

Without loss of generality we take $W > 0$ and $\Delta > 0$. We focus on the physically relevant regime where, $\Delta < W$. To show the twofold degeneracy for the non-interacting case that arises from Majorana zero modes, first a Majorana operator is defined that is associated with each end of the chain at $j = 1$ on the left and $j = 2N$ on the right. The operators are given by

$$\gamma_{\mathrm{R}} = A_{\mathrm{R}}\sum_{n=0}^{\lfloor\frac{N}{2}\rfloor}\left(-\frac{W-\Delta}{W+\Delta}\right)^n(a_{2N-2n} + a_{2N-2n}^\dagger) \tag{3.2}$$

$$\gamma_{\mathrm{L}} = A_{\mathrm{L}}\sum_{n=1}^{\lfloor\frac{N}{2}\rfloor}\left(-\frac{W-\Delta}{W+\Delta}\right)^n(a_{2n-1} + a_{2n-1}^\dagger), \tag{3.3}$$

where, A_{L} and A_{R} are normalization constants that are defined so that $(\gamma_{\mathrm{L}})^2 = (\gamma_{\mathrm{R}})^2 = 1$. These operators are exponentially localised at the ends and have the decay constant

$$\nu = \log\sqrt{\frac{W+\Delta}{W-\Delta}}. \tag{3.4}$$

The Majorana operators have the commutation relation

$$\{\gamma_\alpha, \gamma_\beta\} = 2\delta_{\alpha,\beta}, \tag{3.5}$$

where, α and β stand for left or right. This follows in a very straightforward way from the property that $(\gamma_\alpha)^2 = 1$. The Majorana operators at the end of the chain commute with the non-interacting Hamiltonian. This is shown in detail in

Appendix C. From these results, fermionic creation and annihilation operators can be defined in terms of the Majorana operators that also commute with the Hamiltonian. They are given by

$$c = \gamma_{\mathrm{L}} + i\gamma_{\mathrm{R}}, \tag{3.6}$$

where,

$$c^2 = 0, \quad \{c, c^\dagger\} = 1, \tag{3.7}$$

and hence, $[H_0, c] = 0$ and $[H_0, c^\dagger c] = 0$. The orbital in which $c^\dagger$ creates a particle will be called the c-orbital. H and $c^\dagger c$ can be diagonalized simultaneously, so that every eigenstate of H can be labelled by whether the c-orbital is empty or filled. Furthermore since c and $c^\dagger$ change the occupation of this orbital and commute with H, for every state where the orbital is empty with energy E, there is another state at energy E where the orbital is filled, and vice versa. In Chapter 2 we have seen that the ground state of the non-interacting system with a junction is not two, but fourfold degenerate. This further degeneracy is associated with another zero energy orbital. This time it is localized at the junction, rather than being composed of two Majorana operators that are localized at opposite ends of the wire.

As mentioned in Chapter 1, it has been proven that the twofold spectral degeneracy of the system without a junction is present after the addition of particle hole symmetric interactions [25]. The proof was done by the construction of dressed Majorana fermion operators. These are operators that are complicated multinomials of fermionic operators rather than the linear combinations that appear in the non-interacting counterparts given in Eq. 3.2. The dressed operators are Hermitian, obey the Majorana commutation relations in Eq. 3.5, still commute with the Hamiltonian and decay exponentially into the bulk. This proof by construction shows that the twofold degeneracy throughout the spectrum discussed before is preserved as long as there is a bulk gap.

3.1 MZMs in the presence of interactions

We are finally ready to study the interacting system containing a Josephson junction (Eq. 1.6) using DMRG. We study both attractive and, the more physical, repulsive

interactions given by $U < 0$ and $U > 0$, respectively. As stated before, without loss of generality, we take W, $\Delta > 0$, and consider the physically relevant regime $\Delta < W$ where the superconducting gap is less than the bandwidth. The XYZ chain has a gap for all values of U except at the critical point, where $|U| = W + \Delta$. This means that according to the result derived by Fendley [25], there should be at least a twofold degeneracy for all values except at the critical points. There are two phases that we study, the intrinsically gapped phase is where $|U| > W + \Delta$ and the physics of the system is governed mostly by the intrinsic interactions between the fermions in the 1D wire. Here it is expected that only a two fold degeneracy will be observed because the term in the XYZ model governed by J_z will dominate. For very large J_z compared to J_x and J_y, the chain will reduce to the Ising model and so it will have two fold degeneracy. This can only change after a phase transition, which occurs when $J_z = \text{Max}\{J_x, J_y\}$. This is the transition to the extrinsically gapped phase. The extrinsically gapped phase, $|U| < W + \Delta$, is where the dominant interaction is the pairing between the fermions in the wire that is induced by the proximity effect from the s-wave superconductor with which it is in contact.

The DMRG program was used to calculate the first 12 eigenenergies for a system with 41 sites on either side of the junction. A single sweep of finite system DMRG was performed and 56 states were kept. The parameters chosen were $\Delta/W = 0.2$ and $U/(W + \Delta) \in (-1.67, 1.67)$. The calculation was limited to only a few excited states as the targetting and state averaging takes an increasing amount of time for each state. Furthermore, as higher energy states are calculated the accuracy of the program decreases for a given number of kept states.

The first twelve energy levels are depicted in Fig. 3.1 for four choices of $U/(W + \Delta)$ in the range studied. Two values were chosen in both the intrinsically and extrinsically gapped phases. For $U < 0$, which corresponds to attractive, intrinsic electron-electron interactions, the figure shows that the system displays twofold degeneracy throughout the spectrum in the intrinsically gapped phase Fig. 3.1a and a fourfold degeneracy in the entire spectrum in the extrinsically gapped phase Fig. 3.1b.

The closing of the gap for $U < 0$ is depicted in Fig. 3.2a. In this figure, the

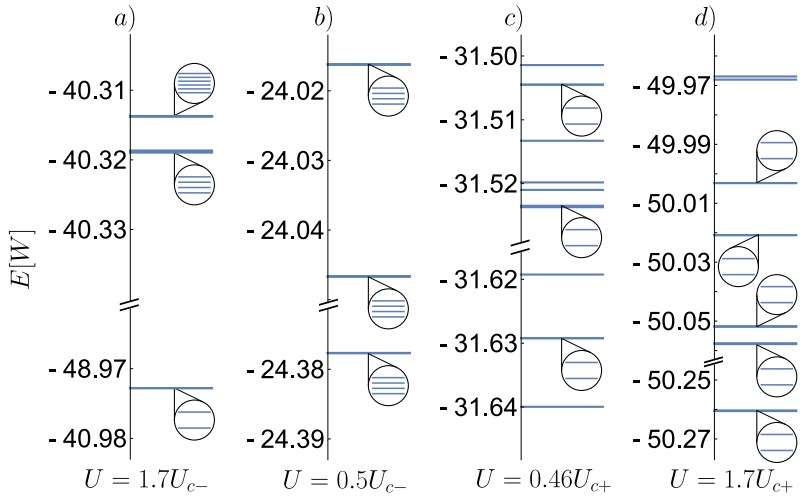

Figure 3.1: The first 12 eigenenergies of the wire with a Josephson junction with a π phase difference across it. The system on either side of the junction has 41 sites and 56 states are kept at each DMRG truncation step. Four values of U are shown in terms of $U_{c\pm} = |W + \Delta|$. The two panels in the centre show the behaviour for the intrinsically gapped phase and the outer two panels show the extrinsically gapped phase. Finite size effects are more apparent for $U > 0$ as shown by the degeneracy of the ground and excited states lifting.

difference from the first seven excited states to the ground state is depicted for various values of $U/(W + \Delta)$. The data points are joined to guide the eye. The fourfold degeneracy survives very close to the critical point $U = W + \Delta$ after which point there is a sharp transition to twofold degeneracy throughout the spectrum. This figure shows that the gap closes linearly in $U/(W + \Delta)$. Thus, for attractive interactions, the 4π Josephson effect survives within the extrinsically gapped phase under attractive particle hole symmetric electron-electron interactions. In the intrinsically gapped phase, as expected, only two fold degeneracy remains.

The two panels on the right of Fig. 3.1 show the effect of repulsive interactions on the degeneracies. It can be seen that in the extrinsically gapped phase, Fig. 3.1c, the ground state is not degenerate and there is no clear pattern for any other degeneracies. We therefore need to do further work to determine whether fourfold degeneracy is being obscured by finite size corrections, or whether something else is going on in the extrinsically gapped repulsive case. In the intrinsically gapped phase, Fig. 3.1d, a twofold degeneracy throughout the spectrum is recovered once U is made large enough.

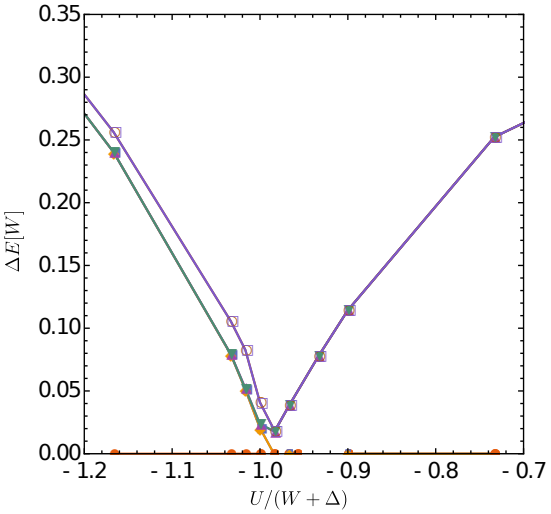

(a) The difference of the first eight eigenenergies from the ground state when U$\in (-1.2, -0.7)$. The lines serve as a guide for the eye. The finite size effects for $U < 0$ are not very noticeable even close to the gap closing.

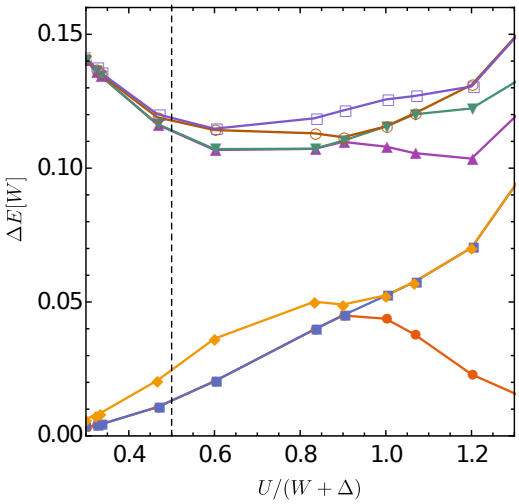

(b) The difference of the first eight eigenenergies from the ground state when U$\in (0.3, 1.3)$. The lines serve as a guide for the eye. The dashed line at $U/(W+\Delta)$ represents the point in parameter space where finite size scaling was performed.

In order to understand if finite size effects are obscuring the degeneracy, we first look at how the gap closes at the critical point. The closing of the gap for $U > 0$ is depicted in Fig. 3.2b. It is known that the gap closes quadratically in $U/(W+\Delta)$ for repulsive interactions [37]. Thus, it is expected that finite size effects would be more pronounced for positive values of $U/(W+\Delta)$. This is because there is a larger range of values for which the gap is small. The data in Fig. 3.2b is consistent with this.

Finite size scaling was performed in order to determine if the size of the gap for $U > 0$ is the only contributing factor to the lifting of the degeneracies. This was done by varying $2N$, the length of the full chain including the junction, from 82 sites to 162 sites at the critical point, $U/(W+\Delta) = 1$, and for $U/(W+\Delta) = 0.5$. The latter choice of repulsion is shown by a dotted line in Fig 3.2b. At these points, the first four energies were calculated. It was found that at the critical point, the difference between the ground state energy and the first excited state decays as $1/N$. This is the expected behaviour when there is no gap. When $U/(W+\Delta) = 0.5$, the difference between the ground state and first three excited states decays exponentially. This is depicted in Fig 3.3. It suggests that for an infinite system, that is in the absence of finite size effects, fourfold degeneracy

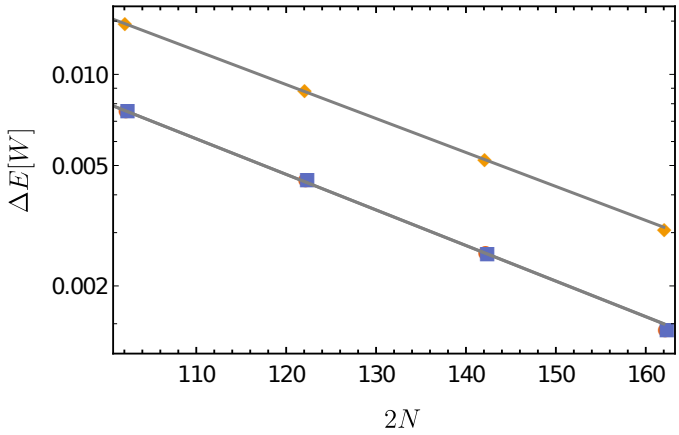

Figure 3.3: The difference from the ground state energy for the first four excited states was calculated as a function of increasing system size. The decay was fit with an exponential function of N depicted by the grey lines.

will be present in the extrinsically gapped phase and two fold in the intrinsically gapped phase. Thus, for infinite systems the 4π Josephson effect survives in the repulsive, extrinsically gapped phase.

From these results we cannot determine if the significant finite size corrections that we see in the extrinsically gapped, repulsive case, are merely a manifestation of the expected gap reduction or if a more subtle interaction effect is at play. In other words, how do the finite size corrections in the interacting system behave as compared to a non-interacting system with the same gap? To answer this question, the following analysis of the results in Fig. 3.3 is done. Through fitting, we extracted the exponential decay rate of finite size corrections at U/(W+Delta)=0.5, and found $\sim (0.95)^N$. We then set out to determine which value of Δ/W would produce the same decay in a non-interacting system. It must be noted that the expected decay in the non-interacting system from Eq. 3.4 is $[(W+\Delta)/(W-\Delta)]^{(N/2)}$. The value of Δ obtained from the fit is then 0.054W. This value is used to calculate the first 5 energies of a non-interacting chain with 82 sites and a Josephson Junction in the middle. The difference in energy between the first state in the band (the fifth energy calculated) and the ground state was found to be 0.081W. The same difference in energy in the interacting Josephson junction system with 82 sites is 0.116W. That is, for the same rate of decay of finite size effects, the non-interacting system has a much smaller gap than the interacting system.

Finite size corrections decay faster if the gap of the non-interacting system is increased. Thus, we arrive at the important conclusion: if two systems with the same gap are compared, one with repulsive interactions, and one without, finite size corrections will decay more slowly as a function of wire length in the interacting system than in the non-interacting system. This is an unambiguous signal that repulsive interactions frustrate superconductivity in a way that a mean-field description cannot account for.

To summarize, in this chapter we have seen the following. For $U < -(W + \Delta)/2$ the ground state and excited states we looked at are clearly twofold degenerate at worst. For $-(W + \Delta)/2 < U < 0$, both the ground state and the excited states we looked at are fourfold degenerate. The presence of quasiparticles in the bulk can therefore not spoil the 4π Josephson effect, as would be the case if only the ground state was fourfold degenerate. For $0 < U < (W + \Delta)/2$, and a system size of 82 sites, degeneracies are hard to discern. We have performed a finite size scaling analysis and could clearly show that the ground state degeneracy of the infinite system is fourfold. We expect the same to be true for the excited states. We showed that finite size corrections decay more slowly in a system with repulsive interactions than in one with the same gap but no interactions. The enhanced finite size corrections in the system with repulsive interactions are therefore not simply due to the reduction of the gap. We were also able to show that the gap of the infinite system closes at $U = (W + \Delta)/2$ as expected. For $U > (W + \Delta)/2$ we could again observe the at worst twofold degeneracy of the ground state and excited states.

4 Conclusions

There are many systems in condensed matter physics that can be well described if interactions are approximated by an effective mean field theory. However, if interactions are not effectively screened by the electron plasma, a full many body description may be required to obtain an accurate understanding of the behaviour of the system. DMRG is a method that is used to describe the behaviour of strongly correlated many body systems. In this dissertation, it has been applied to a minimal system to determine the effects of short range particle hole symmetric interactions. DMRG was chosen as it can be used to study large systems to a high level of precision at a relatively low computational cost. The system we study is a gapped system with local interactions and DMRG approximates such systems well. For these reasons it is a common numerical method for the study of strongly correlated systems.

The implementation of a DMRG program is non-trivial and there are many open source programs available. However, as it was one of the aims of this work to understand this method, a DMRG program was developed from scratch. The methodology given in this thesis complements the many excellent reviews on this topic by expanding on the basic practical details of writing such a program. The program that was developed was checked against exact calculations and we found that it approximated the behaviour well. This program was then used to study a non-trivial albeit minimal system.

More specifically, we studied a one-dimensional nanowire with strong spin-orbit coupling in contact with a bulk superconductor. The electrons in this wire are effectively spinless and thus have p-wave like pairing between them. Such a system

has a twofold degeneracy throughout the spectrum as a result of a zero energy orbital that is localised at the ends of the chain. It is known that this degeneracy is robust to the addition of particle-hole symmetric interactions. Thus, interactions are not a source of quasiparticle poisoning of these orbitals. This is an important result for the production of self correcting quantum memory.

We allowed the order parameter to have a spatial dependence by introducing a Josephson junction in the centre of the wire. In such a system the unusual 4π Josephson effect has been observed which may be useful to detect Majorana fermions. When the phase difference between the two sides of the junction is π, there is an additional zero energy orbital localised at the junction. This gives rise to a four fold degeneracy throughout the spectrum when no interactions are present. DMRG was used to show that this is also the case in interacting systems as long as the system is large enough and interactions are not too strong. Thus, there is no quasiparticle poisoning of the 4π Josephson effect.

Additionally, when repulsive interactions were studied, it was found that finite size effects caused the lifting of degeneracies. This is an important result as there are limitations on how large systems of this kind can be made before disorder destroys the topological properties of the wire which are essential for its applications to quantum error correction. An analysis of these finite size effects was performed and we found that the finite size corrections decay slower than expected when repulsive interactions are present. Thus, we conclude that repulsive interactions frustrate superconductivity in a way that cannot be accounted for if a mean field approach is used. Hence, the use of DMRG uncovered an effect that would not be accounted for if only an infinite system or mean field approach was considered.

References

[1] U. Schollwöck, "The density-matrix renormalization group," *Rev. Mod. Phys.* **77** (Apr., 2005) 259–315.

[2] T. Giamarchi, "One-dimensional physics in the 21st century," *C. R. Phys.* **17** no. 3, (2016) 322 – 331. Physique de la matière condensée au XXIe siècle: l'héritage de Jacques Friedel.

[3] J. Boeyens and I. Snyman, "Fortran implementation of DMRG for a Heisenberg spin chain with a Josephson junction," Apr., 2020. `https://doi.org/10.5281/zenodo.3757159`.

[4] U. Schollwöck, "The density-matrix renormalization group in the age of matrix product states," *Ann. Phys.* **326** no. 1, (2011) 96 – 192. January 2011 Special Issue.

[5] J. Boeyens and I. Snyman, "Zero-energy quasiparticles in an interacting nanowire containing a topological Josephson junction," `arXiv:2003.03276 [cond-mat.mes-hall]`.

[6] N. N. Bogoliubov, "A new method in the theory of superconductivity," *Sov. Phys. JETP 7* **34** no. 1, (July, 1958) 41–46.

[7] E. M. Stoudenmire, J. Alicea, O. A. Starykh, and M. P. Fisher, "Interaction effects in topological superconducting wires supporting Majorana fermions," *Phys. Rev. B* **84** (Jul., 2011) 014503.

[8] R. Thomale, S. Rachel, and P. Schmitteckert, "Tunneling spectra simulation of interacting Majorana wires," *Phys. Rev. B* **88** (Oct., 2013) 161103.

[9] E. Sela, A. Altland, and A. Rosch, "Majorana fermions in strongly interacting helical liquids," *Phys. Rev. B* **84** (Aug, 2011) 085114.

[10] S. Gangadharaiah, B. Braunecker, P. Simon, and D. Loss, "Majorana edge states in interacting one-dimensional systems," *Phys. Rev. Lett.* **107** (Jul, 2011) 036801.

[11] Y. Chan, C. Chiu, and K. Sun, "Multiple signatures of topological transitions for interacting fermions in chain lattices," *Phys. Rev. B* **92** (Sep, 2015) 104514.

[12] R. Shankar, "Renormalization-group approach to interacting fermions," *Rev. Mod. Phys.* **66** (Jan, 1994) 129–192. https://link.aps.org/doi/10.1103/RevModPhys.66.129.

[13] M. Leijnse and K. Flensberg, "Introduction to topological superconductivity and Majorana fermions," *Semicond. Sci.Tech.* **27** no. 12, (Nov., 2012) 124003.

[14] C. Beenakker, "Search for Majorana fermions in superconductors," *Annu. Rev. Condens. Matter Phys.* **4** no. 1, (2013) 113–136.

[15] Y. Oreg, G. Refael, and F. von Oppen, "Helical liquids and Majorana bound states in quantum wires," *Phys. Rev. Lett.* **105** (Oct, 2010) 177002.

[16] A. Y. Kitaev, "Unpaired Majorana fermions in quantum wires," *Phys.-Uspekhi* **44** no. 10S, (Oct., 2001) 131–136.

[17] J. Alicea, "New directions in the pursuit of Majorana fermions in solid state systems," *Reports on Progress in Physics* **75** no. 7, (Jun, 2012) 076501.

[18] S. D. Sarma, M. Freedman, and C. Nayak, "Majorana zero modes and topological quantum computation," *Npj Quantum Inf.* **1** no. 15001, (Oct., 2015) 2056–6387.

[19] X.-G. Wen, "Colloquium: Zoo of quantum-topological phases of matter," *Rev. Mod. Phys.* **89** (Dec, 2017) 041004. https://link.aps.org/doi/10.1103/RevModPhys.89.041004.

[20] P. Bonderson and C. Nayak, "Quasi-topological phases of matter and topological protection," *Phys. Rev. B* **87** (May, 2013) 195451. https://link.aps.org/doi/10.1103/PhysRevB.87.195451.

[21] J. Klassen and X. Wen, "Topological degeneracy (Majorana zero-mode) and 1+1D fermionic topological order in a magnetic chain on superconductor via spontaneous $\mathbf{Z}_2^f$ symmetry breaking," *Journal of Physics: Condensed Matter* **27** no. 40, (Sep, 2015) 405601.

[22] A. S. Jermyn, R. S. K. Mong, J. Alicea, and P. Fendley, "Stability of zero modes in parafermion chains," *Phys. Rev. B* **90** (Oct, 2014) 165106.

[23] J. Alicea and P. Fendley, "Topological phases with parafermions: Theory and blueprints," *Annual Review of Condensed Matter Physics* **7** no. 1, (2016) 119–139.

[24] K. Kawabata, R. Kobayashi, N. Wu, and H. Katsura, "Exact zero modes in twisted kitaev chains," *Phys. Rev. B* **95** (May, 2017) 195140.

[25] P. Fendley, "Strong zero modes and eigenstate phase transitions in the XYZ/interacting Majorana chain," *J. Phys. A* **49** no. 30, (Jun., 2016) 30LT01.

[26] P. Jordan and E. Wigner, "Über das Paulische Äquivalenzverbot," *Z. Physik* **47** (Sep., 1928) .

[27] K. G. Wilson, "The renormalization group: Critical phenomena and the Kondo problem," *Rev. Mod. Phys.* **47** (Oct., 1975) 773–840.

[28] R. Bulla, T. A. Costi, and T. Pruschke, "Numerical renormalization group method for quantum impurity systems," *Rev. Mod. Phys.* **80** (Apr., 2008) 395–450.

[29] S. R. White and R. M. Noack, "Real-space quantum renormalization groups," *Phys. Rev. Lett.* **68** (Jun., 1992) 3487–3490.

[30] S. R. White, "Density-matrix algorithms for quantum renormalization groups," *Phys. Rev. B* **48** (Oct., 1993) 10345–10356.

[31] D. S. R. B. Lehoucq and C. Yang, *ARPACK Users' Guide: Solution of Large-scale Eigenvalue Problems with Implicitly Restarted Arnoldi Methods*. Society for Industrial and Applied Mathematics, 1st ed., 1998.

[32] S. R. White, "Density matrix formulation for quantum renormalization groups," *Phys. Rev. Lett.* **69** (Nov., 1992) 2863–2866.

[33] J. J. Dorando, J. Hachmann, and G. K. Chan, "Targeted excited state algorithms," *J. Chem. Phys.* **127** (2007) 084109.

[34] L. Fu and C. L. Kane, "Josephson current and noise at a superconductor/quantum-spin-hall-insulator/superconductor junction," *Phys. Rev. B* **79** (Apr, 2009) 161408.

[35] D. Laroche, D. Bouman, D. J. van Woerkom, A. Proutski, C. Murthy, C. Pikulin, Dmitry I.and Nayak, J. van Gulik, Ruben J. J.and Nygård, P. Krogstrup, L. P. Kouwenhoven, and A. Geresdi, "Observation of the 4 π-periodic Josephson effect in indium arsenide nanowires," *Nat. Commun.* **10** (Jan., 2019) 245.

[36] D. I. Pikulin and Y. V. Nazarov, "Phenomenology and dynamics of a Majorana Josephson junction," *Phys. Rev. B* **86** (Oct, 2012) 140504.

[37] A. Alexandradinata, N. Regnault, C. Fang, M. J. Gilbert, and B. A. Bernevig, "Parafermionic phases with symmetry breaking and topological order," *Phys. Rev. B* **94** (Sep., 2016) 125103.

A Properties of the Pauli matrices

The following definitions of the Jordan-Wigner transformations are restated here for ease of reference

$$\begin{aligned}\sigma_j^x &= \prod_{k=1}^{j-1}(2n_k - 1)(a_j + a_j^\dagger) \\ \sigma_j^y &= \prod_{k=1}^{j-1}(2n_k - 1)i(a_j - a_j^\dagger) \\ \sigma_j^z &= 2n_j - 1. \end{aligned} \tag{A.1}$$

The properties that will be proved are

$$(\sigma_j^x)^2 = (\sigma_j^y)^2 = (\sigma_j^z)^2 = 1 \tag{A.2}$$

$$\sigma_j^x \sigma_j^y = i\sigma_j^z \tag{A.3}$$

$$[\sigma_j^x, \sigma_k^y] = [\sigma_j^x, \sigma_k^z] = [\sigma_j^y, \sigma_k^z] = 0, \quad \text{if } \ j \neq k. \tag{A.4}$$

First consider $(\sigma_j^x)^2$, since $[n_l, a_m] = 0$, when $l \neq m$.

$$\begin{aligned}
(\sigma_j^x)^2 &= \prod_{k=1}^{j-1}(2n_k - 1)(a_j + a_j^\dagger)\prod_{k=1}^{j-1}(2n_k - 1)(a_j + a_j^\dagger) \\
&= \prod_{k=1}^{j-1}(2n_k - 1)^2(a_j + a_j^\dagger)^2 \\
&= (a_j + a_j^\dagger)^2 \\
&= a_j a_j + a_j^\dagger a_j^\dagger + a_j a_j^\dagger + a_j^\dagger a_j. \\
&= 1 - a_j^\dagger a_j + a_j^\dagger a_j. \\
&= 1. \qquad \text{(A.5)}
\end{aligned}$$

The result for $(\sigma_j^y)^2$ follows similarly. The proof of Eq. A.2 is concluded by

$$\begin{aligned}
(\sigma_j^z)^2 &= (2n_j - 1)^2 \\
&= 4n_j^2 - 4n_j + 1 \\
&= 1, \qquad \text{(A.6)}
\end{aligned}$$

since $n_j^2 = n_j$.

Next, the result for Eq. A.3 follows from similar manipulations,

$$\begin{aligned}
\sigma_j^x \sigma_j^y &= i\prod_{k=1}^{j-1}(2n_k - 1)(a_j + a_j^\dagger)\prod_{k=1}^{j-1}(2n_k - 1)(a_j - a_j^\dagger) \\
&= i(a_j + a_j^\dagger)(a_j - a_j^\dagger) \\
&= i(a_j a_j - a_j^\dagger a_j^\dagger - a_j a_j^\dagger + a_j^\dagger a_j) \\
&= i(a_j^\dagger a_j - (1 - a_j^\dagger a_j)) \\
&= i(2n_j - 1) \\
&= i\sigma_j^z. \qquad \text{(A.7)}
\end{aligned}$$

Finally for the commutation relations in Eq. A.4 consider first $[\sigma_j^x, \sigma_k^y]$, $j \neq k$. We

consider only the case when $j < k$ since the proof for $j > k$ is similar.

$$[\sigma_j^x, \sigma_k^y] = \sigma_j^x \sigma_k^y - \sigma_k^y, \sigma_j^x \tag{A.8}$$

The term $\sigma_j^x \sigma_k^y$ is given in terms of fermionic operators as

$$\begin{aligned}\sigma_j^x \sigma_k^y =& \prod_{l=1}^{j-1} (2n_l - 1)^2 (a_j + a_j^\dagger)(2n_j - 1)(2n_{j+1} - 1) \dots (2n_{k-1} - 1)\ i(a_k - a_k^\dagger) \\ =& (a_j - a_j^\dagger)(2n_{j+1} - 1) \dots (2n_{k-1} - 1)\ i(a_k - a_k^\dagger).\end{aligned} \tag{A.9}$$

Then,

$$\begin{aligned}\sigma_k^y \sigma_j^x =& (2n_j - 1)(2n_{j+1} - 1) \dots (2n_{k-1} - 1)\ i(a_k - a_k^\dagger)(a_j + a_j^\dagger) \\ =& (2n_{j+1} - 1) \dots (2n_{k-1} - 1)\ i(a_k - a_k^\dagger)(2n_j - 1)(a_j + a_j^\dagger) \\ =& (2n_{j+1} - 1) \dots (2n_{k-1} - 1)\ i(a_k - a_k^\dagger)(-a_j + a_j^\dagger) \\ =& (2n_{j+1} - 1) \dots (2n_{k-1} - 1)(a_j + a_j^\dagger)\ i(a_k - a_k^\dagger) \\ =& \sigma_j^x \sigma_k^y.\end{aligned} \tag{A.10}$$

therefore the commutator is zero. Next the commutator $[\sigma_j^x, \sigma_k^z]$, is given by

$$\begin{aligned}[\sigma_j^x, \sigma_k^z] =& [(2n_1 - 1) \dots (2n_{j-1} - 1)(a_j + a_j^\dagger), (2n_k - 1)] \\ =& 2(2n_1 - 1) \dots (2n_{j-1} - 1)[(a_j + a_j^\dagger), n_k] \\ =& 2(2n_1 - 1) \dots (2n_{j-1} - 1)([a_j, n_k] + [a_j^\dagger, n_k]) \\ =& 2(2n_1 - 1) \dots (2n_{j-1} - 1)(a_j - a_j^\dagger)\delta_{j,k}. \\ =& -2\ i\sigma_j^y \delta_{j,k}.\end{aligned} \tag{A.11}$$

The result for $[\sigma_j^y, \sigma_k^z]$, follows similarly.

B Anti-commutation relation of the BdG operators

First of all, for

$$\{d_k^\dagger, d_k\} = 1, \tag{B.1}$$

since the commutation relations for the fermionic operators a_m and $a_m^\dagger$ ensure that the only non zero contributions are for $\{a_m^\dagger, a_m\} = 1$, we have that

$$\begin{aligned}
&\{\sum_{m=1}^{N} u_{km}a_m + v_{km}a_m^\dagger, \sum_{n=1}^{N} u_{kn}a_n^\dagger + v_{kn}a_n\} \\
&= \sum_{m,n} u_{km}u_{kn}\{a_m, a_n^\dagger\} + v_{km}v_{kn}\{a_m^\dagger, a_n\} \\
&= \sum_{m} u_{km}^2\{a_m, a_m^\dagger\} + v_{km}^2\{a_m^\dagger, a_m\} \\
&= \sum_{m=1}^{N} u_{km}^2 + v_{km}^2.
\end{aligned} \tag{B.2}$$

This condition is met because of the structure of H_{BdG} as shown in Eq. 2.37.

Secondly,

$$\{d_k, d_l\} = 0, \tag{B.3}$$

arises from the orthogonality of the eigenstates of H_{BdG} also given in Eq. 2.37. That is,

$$\{\sum_{m=1}^{N} u_{km}a_m + v_{km}a_m^\dagger, \sum_{n=1}^{N} u_{kn}a_n + v_{kn}a_n^\dagger\} \tag{B.4}$$

$$= \sum_{m,n} u_{km}v_{kn}\{a_m, a_n^\dagger\} + v_{km}u_{kn}\{a_m^\dagger, a_n\} \tag{B.5}$$

$$= \sum_{m} u_{km}v_{km} + v_{km}u_{km} = 0. \tag{B.6}$$

C Commutation of Majorana operators with the non-interacting Hamiltonian

For ease of reference, the Majorana operators and non-interacting Hamiltonian are restated here. The Hamiltonian is

$$\begin{aligned} H_{2N_0} = &- \frac{W}{2}\sum_{j=1}^{2N-1}(a_j^\dagger a_{j+1} + a_{j+1}^\dagger a_j) \\ &+ \frac{\Delta}{2}\sum_{j=1}^{N-1}(a_j a_{j+1} + a_{j+1}^\dagger a_j^\dagger) \\ &- \frac{\Delta}{2}\sum_{j=N+1}^{2N-1}(a_j a_{j+1} + a_{j+1}^\dagger a_j^\dagger) \end{aligned} \tag{C.1}$$

and the Majorana operators for the right and left are

$$\gamma_{\mathrm{R}} = A_{\mathrm{R}}\sum_{n=0}^{\lfloor\frac{N}{2}\rfloor}\Big(-\frac{W-\Delta}{W+\Delta}\Big)^n(a_{2N-2n} + a_{2N-2n}^\dagger) \tag{C.2}$$

and

$$\gamma_{\mathrm{L}} = A_{\mathrm{L}}\sum_{n=1}^{\lfloor\frac{N}{2}\rfloor}\Big(-\frac{W-\Delta}{W+\Delta}\Big)^n(a_{2n-1} + a_{2n-1}^\dagger), \tag{C.3}$$

respectively. The commutation of these operators with the non- interacting Hamiltonian is shown for γ_{L}, the result for the right operator follows in a similar

way. Then, first note that

$$[a_j^\dagger a_{j+1}, a_{2n-1} + a_{2n-1}^\dagger] = -\delta_{j,2n-1} a_{j+1} + a_j^\dagger \delta_{j+1,2n-1}. \tag{C.4}$$

Then consider the following

$$\begin{aligned}
[a_j^\dagger a_{j+1}, \gamma_{\mathrm{L}}] &= A_{\mathrm{L}} \sum_{n=1}^{\lfloor \frac{N}{2} \rfloor} \left(- \frac{W-\Delta}{W+\Delta} \right)^n [\delta_{j+1,2n-1} a_j^\dagger - \delta_{j,2n-1} a_{j+1}] \\
&= A_{\mathrm{L}} \begin{cases} \left(- \frac{W-\Delta}{W+\Delta} \right)^{\frac{j}{2}+1} a_j^\dagger, \ j \text{ even and } j \leq 2\lfloor \frac{N}{2} \rfloor - 2 \\ -\left(- \frac{W-\Delta}{W+\Delta} \right)^{\frac{j+1}{2}} a_{j+1}, \ j \text{ odd and } j \leq 2\lfloor \frac{N}{2} \rfloor - 1 \\ 0, \text{ otherwise.} \end{cases}
\end{aligned} \tag{C.5}$$

Furthermore,

$$\begin{aligned}
[a_j^\dagger a_{j+1} + a_{j+1}^\dagger a_j, \gamma_{\mathrm{L}}] &= [a_j^\dagger a_{j+1}, \gamma_{\mathrm{L}}] - [a_j^\dagger a_{j+1}, \gamma_{\mathrm{L}}]^\dagger \\
&= A_{\mathrm{L}} \begin{cases} \left(- \frac{W-\Delta}{W+\Delta} \right)^{\frac{j}{2}+1} (a_j^\dagger - a_j), \ j \text{ even and } j \leq 2\lfloor \frac{N}{2} \rfloor - 2 \\ \left(- \frac{W-\Delta}{W+\Delta} \right)^{\frac{j+1}{2}} (a_{j+1}^\dagger - a_{j+1}), \ j \text{ odd and } j \leq 2\lfloor \frac{N}{2} \rfloor - 1 \\ 0, \text{ otherwise.} \end{cases}
\end{aligned} \tag{C.6}$$

Then, to perform this calculation in the sum that appears in the Hamiltonian, we first calculate for the sum over j from 1 to $2N$ and then use this result to calculate the sum from 1 to $2N-1$. That is,

$$\begin{aligned}
\left[\sum_{j=1}^{2N} a_j^\dagger a_{j+1} + a_{j+1}^\dagger a_j, \gamma_{\mathrm{L}} \right] =& A_{\mathrm{L}} \sum_{l=1}^{\lfloor \frac{N}{2} \rfloor - 1} \left(- \frac{W-\Delta}{W+\Delta} \right)^{l+1} (a_{2l}^\dagger - a_{2l}) \\
&+ A_{\mathrm{L}} \sum_{l=1}^{\lfloor \frac{N}{2} \rfloor} \left(- \frac{W-\Delta}{W+\Delta} \right)^{l} (a_{2l}^\dagger - a_{2l}),
\end{aligned} \tag{C.7}$$

where, in the first summation we account for even j so, $j = 2l$ and odd in the second, $j = 2l - 1$. Thus,

$$\begin{aligned}\Big[\sum_{j=1}^{2N-1} a_j^\dagger a_{j+1} + a_{j+1}^\dagger a_j, \gamma_{\mathrm{L}}\Big] =& A_{\mathrm{L}} \sum_{l=1}^{\lfloor \frac{N}{2} \rfloor - 1} \Big(- \frac{W-\Delta}{W+\Delta}\Big)^l \Big[- \frac{W-\Delta}{W+\Delta} + 1\Big](a_{2l}^\dagger - a_{2l}) \\ &+ A_{\mathrm{L}} \Big(- \frac{W-\Delta}{W+\Delta}\Big)^{\lfloor \frac{N}{2} \rfloor} (a_{2\lfloor \frac{N}{2} \rfloor}^\dagger - a_{2\lfloor \frac{N}{2} \rfloor}) \\ =& A_{\mathrm{L}} \sum_{l=1}^{\lfloor \frac{N}{2} \rfloor - 1} \Big(- \frac{W-\Delta}{W+\Delta}\Big)^l \Big[- \frac{2\Delta}{W+\Delta}\Big](a_{2l}^\dagger - a_{2l}) \\ &+ A_{\mathrm{L}} \Big(- \frac{W-\Delta}{W+\Delta}\Big)^{\lfloor \frac{N}{2} \rfloor} (a_{2\lfloor \frac{N}{2} \rfloor}^\dagger - a_{2\lfloor \frac{N}{2} \rfloor}). \end{aligned} \tag{C.8}$$

Next, consider the terms that give the super conducting pairing,

$$[a_j a_{j+1}, a_{2n-1} + a_{2n-1}^\dagger] = a_j \delta_{j+1,2n-1} - a_{j+1}\delta_{j,2n-1}. \tag{C.9}$$

Then,

$$[a_j a_{j+1}, \gamma_{\mathrm{L}}] = A_{\mathrm{L}} \begin{cases} \Big(- \frac{W-\Delta}{W+\Delta}\Big)^{\frac{j}{2}+1} a_j, \ j \text{ even and } j \leq 2\lfloor \frac{N}{2} \rfloor - 2 \\ -\Big(- \frac{W-\Delta}{W+\Delta}\Big)^{\frac{j+1}{2}} a_{j+1}, \ j \text{ odd and } j \leq 2\lfloor \frac{N}{2} \rfloor - 1 \\ 0, \text{ otherwise.} \end{cases} \tag{C.10}$$

Furthermore,

$$[a_j a_{j+1} + a_{j+1}^\dagger a_j^\dagger, \gamma_{\mathrm{L}}] = [a_j a_{j+1}, \gamma_{\mathrm{L}}] - [a_j a_{j+1}, \gamma_{\mathrm{L}}]^\dagger \tag{C.11}$$

Then to perform this calculation in the sum that appears in the Hamiltonian, we calculate for the sum over j from 1 to $N-1$ as after this point the order parameter

changes sign. Thus,

$$\Big[\sum_{j=1}^{N-1} a_j a_{j+1} + a_{j+1}^\dagger a_j^\dagger, \gamma_{\rm L}\Big] = -A_{\rm L} \sum_{l=1}^{\lfloor \frac{N}{2} \rfloor - 1} \Big(-\frac{W-\Delta}{W+\Delta}\Big)^{l+1} (a_{2l}^\dagger - a_{2l}) + A_{\rm L} \sum_{l=1}^{\lfloor \frac{N}{2} \rfloor} \Big(-\frac{W-\Delta}{W+\Delta}\Big)^{l} (a_{2l}^\dagger - a_{2l}), \tag{C.12}$$

where, the bounds in the summations arise because if N is odd, $2\lfloor \frac{N}{2} \rfloor - 1 = N-2$ and if N is even, $2\lfloor \frac{N}{2} \rfloor - 1 = N-1$. The commutator can be simplified as follows,

$$\begin{aligned}\Big[\sum_{j=1}^{N-1} a_j a_{j+1} + a_{j+1}^\dagger a_j^\dagger, \gamma_{\rm L}\Big] =& -A_{\rm L} \sum_{l=1}^{\lfloor \frac{N}{2} \rfloor - 1} \Big(-\frac{W-\Delta}{W+\Delta}\Big)^{l} \Big[1 + \frac{W-\Delta}{W+\Delta}\Big] (a_{2l}^\dagger - a_{2l}) \\ &+ A_{\rm L} \Big(-\frac{W-\Delta}{W+\Delta}\Big)^{\lfloor \frac{N}{2} \rfloor} (a_{2\lfloor \frac{N}{2} \rfloor}^\dagger - a_{2\lfloor \frac{N}{2} \rfloor}) \\ =& \frac{2W}{W+\Delta} A_{\rm L} \sum_{l=1}^{\lfloor \frac{N}{2} \rfloor - 1} \Big(-\frac{W-\Delta}{W+\Delta}\Big)^{l} (a_{2l}^\dagger - a_{2l}) \\ &+ A_{\rm L} \Big(-\frac{W-\Delta}{W+\Delta}\Big)^{\lfloor \frac{N}{2} \rfloor} (a_{2\lfloor \frac{N}{2} \rfloor}^\dagger - a_{2\lfloor \frac{N}{2} \rfloor}).\end{aligned} \tag{C.13}$$

We are now ready to calculate the commutator with the full Hamiltonian, which gives,

$$[h_{2N,0}.\gamma_{\rm L}] = \frac{W\Delta - W\Delta}{W+\Delta} A_{\rm L} \sum_{l=1}^{\lfloor \frac{N}{2} \rfloor - 1} \Big(-\frac{W-\Delta}{W+\Delta}\Big)^{l} (a_{2l}^\dagger - a_{2l}) \tag{C.14}$$

$$- \frac{W-\Delta}{2} A_{\rm L} \Big(-\frac{W-\Delta}{W+\Delta}\Big)^{\lfloor \frac{N}{2} \rfloor} (a_{2\lfloor \frac{N}{2} \rfloor}^\dagger - a_{2\lfloor \frac{N}{2} \rfloor}). \tag{C.15}$$

The first term is then zero and the second term vanishes exponentially as N increases. Additionally, the normalisation constant A_{L} is given by

$$\begin{aligned} 1 =& A_{\mathrm{L}}^2 \sum_{m=1}^{\lfloor \frac{N}{2} \rfloor - 1} \sum_{n>m}^{\lfloor \frac{N}{2} \rfloor - 1} \left(- \frac{W-\Delta}{W+\Delta} \right)^{n+m} \{ a_{2m-1} + a_{2m-1}^\dagger, a_{2n-1} + a_{2n-1}^\dagger \} \\ &+ A_{\mathrm{L}}^2 \sum_{m=1}^{\lfloor \frac{N}{2} \rfloor - 1} \left(- \frac{W-\Delta}{W+\Delta} \right)^{2m} (a_{2m-1} + a_{2m-1}^\dagger)^2. \end{aligned} \tag{C.16}$$

The anti-commutator in the first term is zero and $(a_{2m-1} + a_{2m-1}^\dagger)^2 = 1$. Therefore,

$$\begin{aligned} 1 =& A_{\mathrm{L}}^2 \left(\frac{W-\Delta}{W+\Delta} \right)^2 \frac{1 - \left(\frac{W-\Delta}{W+\Delta} \right)^{2\lfloor \frac{N}{2} \rfloor}}{1 - \left(\frac{W-\Delta}{W+\Delta} \right)^2} \\ A_{\mathrm{L}} =& \frac{\sqrt{4W\Delta}}{(W-\Delta)\sqrt{1 - \left(\frac{W-\Delta}{W+\Delta} \right)^{2\lfloor \frac{N}{2} \rfloor}}}. \end{aligned} \tag{C.17}$$